Renewable Energy 208 (2023) 627–644

Contents lists available at ScienceDirect

Renewable Energy

journal homepage: www.elsevier.com/locate/renene

Conceptual design and analysis for a novel parallel configuration-type wave energy converter

Yongxing Zhang [a], Zhicong Huang [a,*], Bowei Zou [a], Jing Bian [b]

[a] Shien-Ming Wu School of Intelligent Engineering, South China University of Technology, Guangzhou, 511442, PR China
[b] School of Civil Engineering, Chongqing University, Chongqing, 400044, PR China

ARTICLE INFO

Keywords:
Ocean wave energy
Wave energy converter
Parallel configuration
Energy conversion

ABSTRACT

Oscillating body wave energy converter (OBWEC) is an essential way to exploit wave energy. Existing OBWECs with a single degree of freedom (DOF) suffer from a low energy conversion ratio. Although this power generation limit of OBWECs can be alleviated by increasing DOF, for the multi-DOF OBWEC, specific structure design guidelines, accurate energy conversion modeling and economic cost-related performance analysis at the conceptual design stage are still missing. To address this gap, this study proposes a novel parallel configuration WEC (PCWEC) with the idea of combining the advantages of multi-DOF OBWEC and parallel structure. The PCWEC energy conversion model is established under irregular wave states. Furthermore, we propose an energy cost-efficiency indicator and perform the performance comparison analysis and simulation experiments. Compared with typical OBWECs, results validate that the proposed PCWEC has the following advantages: (i) a significant power generation increase under the same device scale, (ii) greater optimal output power by power take-off control, and (iii) higher energy cost-efficiency under changing wave states. Such a novel PCWEC design concept improves the current OBWEC's power generation performance and application prospect and offers certain guidance for the future commercial development of OBWECs.

1. Introduction

Although large-scale exploitation and utilization of fossil energy meet the needs for rapid economic and social development, fossil energy's high pollution and non-renewable nature make environmental protection and energy shortage problems increasingly serious [1,2]. As a renewable and clean energy source, wave energy has the advantages of high energy density, wide distribution and ample storage capacity. Wave energy exploited by wave energy converters (WECs) is a promising way of grid-connected power generation. Therefore, WECs are important for green and sustainable development in the future [3,4].

WECs can be divided into oscillating body type, oscillating water column type and overtopping type, according to the basic principles of energy utilization technology [5]. Among them, the oscillating body wave energy converter (OBWEC) has attracted more attention from many researchers worldwide because of its flexible installation position. It can either be fixed on the seabed or float on the sea; thus, it can find wide-range application scenarios, from shallow to deep seawater areas [6]. Classified by the shape and size of the floater as well as the relative incident wave direction, the OBWEC can be divided into point absorber WEC (PAWEC), attenuation WEC (AWEC) and terminator WEC (TWEC). Common concerns of these types of OBWEC include low power generation efficiency and high capital investment to reach a full-scale device, severely hindering the commercial development of OBWEC [7,8].

To develop OBWEC with commercial development potential, relevant scholars have carried out efforts in the following five aspects: geometry parameters optimization, power take-off (PTO) optimization, operation mechanism improvement, the accurate modeling of energy conversion and levelised cost of energy (LCOE) analysis. (1) Geometry parameters optimization plays an important role in the overall performance of the OBWEC. To obtain the optimum geometry parameters of the OBWEC, a series of studies [9–12] take maximizing OBWEC output power as the objective function and utilize optimization algorithms, such as genetic algorithm, direct search methods, gradient-based methods and other methods to solve optimal floating body geometry and dimension. Although these reported schemes can facilitate wave energy absorption, they lose generality, in which no current geometry or dimension outperforms all other geometry or dimensions in all wave states [11,13]. More importantly, regardless of how to optimize the

* Corresponding author.
E-mail addresses: wicmyazzhangyx@mail.scut.edu.cn (Y. Zhang), zhiconghuang@scut.edu.cn (Z. Huang), wizoubowei@mail.scut.edu.cn (B. Zou), bian.jing@cqu.edu.cn (J. Bian).

https://doi.org/10.1016/j.renene.2023.03.086
Received 10 July 2022; Received in revised form 8 February 2023; Accepted 19 March 2023
Available online 24 March 2023

Abbreviations

WEC	Wave energy converter
OBWEC	Oscillating body WEC
PCWEC	Parallel configuration WEC
DOF	Degree of freedom
PTO	Power take-off
PAWEC	Point absorber WEC
AWEC	Attenuation WEC
TWEC	Terminator WEC
HDE	Hydrodynamic efficiency
PGE	Power generation efficiency

geometric parameters, the current OBWECs are affected by the single DOF operation mode and can only absorb wave energy in a single direction, which severely limits their output power. That is, the optimized structure of OBWEC based on geometry or dimensions is not necessarily guaranteed to meet the preset energy production requirements in the random ocean wave state. (2) Optimizing the PTO is an important method to improve the power generation efficiency of OBWEC. Different from geometric parameter optimization, this optimization method can be adjusted according to different wave states. More specifically, it makes the frequency of OBWEC close to the wave frequency by adjusting the damping coefficient of PTO and thus realizes the extraction of the maximum power generation using resonance [9,14]. At present, some proposed PTO control strategies, such as reactive control [15,16], latch control [17] and other intelligent control [18,19], can track the point of maximum power output and improve the power generation efficiency of OBWEC. However, similar to the research gap of geometric parameter optimization, the current OBWEC's output power obtained by optimizing the PTO is also severely limited by its single DOF operating mode [20,21]. Therefore, rather than optimizing the PTO, we need to change the operation mechanism of the current OBWEC and make it can absorb wave energy in multiple directions, increasing the upper limit of its power generation. (3) As previously stated, the operating mechanism of OBWEC determines the upper limit of wave energy captured during the energy conversion and plays a decisive role in the amount of power generation. Thus, some scholars presented the concept of a multi-DOF WEC and pointed out that the hydrodynamic performance and energy utilization rate of typical OBWEC can be improved by increasing the DOF [6,22,23]. Based on this concept, a few different configurations of multi-DOF WECs were designed and analyzed. Reference [24] proposed a buoy WEC with a heave, surge and pitch DOFs and indicated that the power absorption of three-DOF buoy WEC is much larger than that of the single-DOF buoy WEC. Reference [21] designed a six-DOF WEC based on the Stewart-Gough platform. Compared with traditional point absorber WECs, the proposed WEC structure can improve the wave energy utilization rate substantially. Reference [25] designed a novel OBWEC, which uses a 4-bar mechanism to capture heave motion and a two-DOF spherical hinge to capture pitch and roll motion. Although these reported schemes enhanced the power generation production substantially, they are not easy to suit for large-scale promotion and application because of a lack of a specific design guideline that comprehensively considers the wave motion characteristics and energy machinery requirements in the design process. (4) The energy conversion modeling of OBWEC includes kinematic response and dynamic response, which lay the important foundation for performance analysis, optimization control and structure parameters optimization in the OBWEC's development process. At present, energy conversion modeling methods of OBWEC include the potential flow, time domain analysis and frequency domain analysis [26]. Based on these methods, related scholars [27–29] construct the models of a series of single-DOF OBWECs, such as PAWEC, AWEC and TWEC. However, relatively few modeling works are on multi-DOF OBWEC. Current research [21,30–32] lacks accurate analysis for the dynamic response of the multi-DOF OBWEC under irregular wave states, further hindering the subsequent research and development of multi-DOF OBWEC. (5) LCOE represents the minimal price paid for the generated power from the device to finance the project cost and can evaluate the economic cost of a power generation system throughout its life cycle [33,34]. Thus, it is widely used in the wave power generation industry to analyze the application potential of different WECs [35]. At present, several different approaches are used to define the WEC's LCOE [33,36,37]. However, the definition given by the International Energy Agency and the Nuclear Energy Agency is usually used as the standard. It is the sum of the total cost of the initial investment, annual operating and maintenance costs; annual fuel and carbon costs; and the cost of decommissioning. However, these detailed cost parameters are relatively scarce because wave power generation technology is not yet fully mature, and successful commercial development has a few cases. Thus, the LCOE of an OBWEC with multi-DOF in the conceptual design stage is difficult to analyze, which also implies that we need to design a more applicable economic cost indicator to evaluate the development potential of multi-DOF OBWEC in the early design stage.

Based on the analysis of the research status in the above five aspects, the existing research gaps can be summarized as follows. Although the power generation upper limit of the current single-DOF OBWEC can be improved substantially by increasing DOF, for the OBWEC with multi-DOF, there remains a lack of specific structure design guidelines, accurate energy conversion modeling and economic cost-related performance analysis at the conceptual design stage. Thus, the present study designs a novel parallel configuration WEC (PCWEC) structure, which is inspired by the concept of multi-DOF OBWEC and parallel mechanical structural characteristics. Moreover, to examine the performance of the proposed PCWEC structure, we construct PCWEC's energy conversion model in the irregular wave and compare the performance of PCWEC with three typical OBWECs under different PTO damping coefficients and wave states. Specifically, the main contributions of this study are as follows:

(1) A novel structure design idea that combines the advantages of multi-DOF OBWEC and parallel structure is proposed, which provides the solution for improving the commercial development potential of the current OBWEC.
(2) The PCWEC energy conversion model is established under irregular wave states, which provides important guidance for the mathematical modeling of this type of OBWEC with multi-DOF.
(3) An energy cost-efficiency index that integrates investment cost and power generation efficiency is defined, which is convenient for evaluating the commercial development potential of different OBWECs in the conceptual design stage.
(4) The performance of PCWEC under different PTO parameters and different wave states is analyzed, providing a deeper insight into the energy conversion of this type of OBWEC.

The remainder of this paper is structured as follows. Section II introduces detailed design concepts and processes. Section III systematically constructs the energy conversion model in irregular wave states to analyze further the energy conversion characteristics of the proposed PCWEC. In addition, we propose an energy cost-efficiency indicator that can create a quantitative relationship between investment cost and the power generation efficiency of OBWECs under different wave states to evaluate the development potential of PCWEC and other OBWECs. Sections IV and V carry out performance comparison analysis and simulation verification. Finally, Section VI concludes this study.

2. Conceptual design

The OBWECs with multi-DOF have a higher energy utilization rate. Moreover, the random and large thrust characteristics of ocean waves

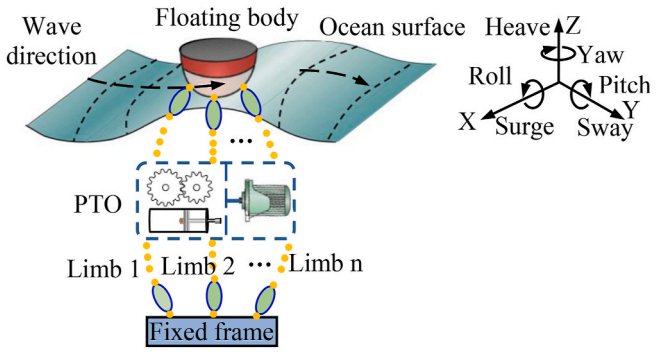

Fig. 1. The basic overall structure of PCWEC.

Table 1
Comparison of parameters of different OBWECs [6].

Name	Category	Location	Data	HDE (%)	Scale (m)	Capacity (Kw)
AquaBuoy	Point absorber	Canada	2000	20	6	250
Wavebob	Point absorber	Ireland	2007	40	15	1000
Pelamis	Attenuator	UK	2007	15	150	750
DEXA	Attenuator	Denmark	2011	8	22	160
Biowave	Terminator	Australia	2008	45	16	250
Oyster	Terminator	UK	2005	40	18	315

require higher reliability for OBWEC structures. To meet the requirements of the above two essential points, we are inspired by the multi-DOF WEC's operation principles and the parallel mechanism's good characteristics, such as kinematic characteristics of multiple DOF and structural characteristics of high stiffness and strong load capacity [38–41] and propose the operation mechanism of PCWEC (See Fig. 1). The PCWEC consists of the floating body, multi limbs, PTO and a fixed frame. When waves flow through the PCWEC, the floating body starts to oscillate erratically in six directions: heave, surge, sway, yaw, pitch and roll and force the *n* limbs to move, thereby driving the PTO to generate electricity. This section concretizes the abstract operational requirements for PCWEC into the structural design of the floating body, limbs and PTO and combines each component organically to obtain the PCWEC with a higher energy utilization rate, reliability and adaptability.

2.1. Floating body design

DOF selection is the first step in designing a floating body. Theoretically, a configuration with many DOF will make the wave energy absorption more adequate for OBWEC. However, considering the sustainability of wave energy absorption, the motion of the floating body should be reciprocating to achieve continuous power generation. The three directions of sway, surge and yaw for an axisymmetric floating body have no restoring force (moment). The heave, surge and pitch directions have a restoring force (moment) that can push the axisymmetric floating body back to the equilibrium position [25]. Thus, three DOFs of heave, pitch and roll should be selected, and other DOFs should be restricted.

The second step is designing the floating body's shape. We draw on the OBWEC engineering prototype tested at sea to achieve it. The specific OBWEC types and corresponding parameters are shown in Table 1. In comparison, the attenuated WEC has the lowest hydrodynamic efficiency (HDE) and the largest scale, and the point absorption type and the terminator type have their advantages. Therefore, we chose to design the PCWEC's floating body concerning the point absorption and terminator float types.

Furthermore, Table 2 shows the floating body's general arrangement patterns and shapes for the point absorber WEC and terminator WEC. Among them, the principal axis of the point absorber WEC is perpendicular to the ocean surface, absorbing the wave energy from the heave direction, whereas the principal axis of the terminator WEC is perpendicular to the wave direction, absorbing the wave energy from the pitch direction. The single floating body in Table 2 cannot absorb the wave energy in the three directions of heave, pitch and roll. Here, we combine the above two types of floating bodies to complete the energy absorption requirements.

Table 2
Arrangement patterns and shapes for the OBWECs [42–53].

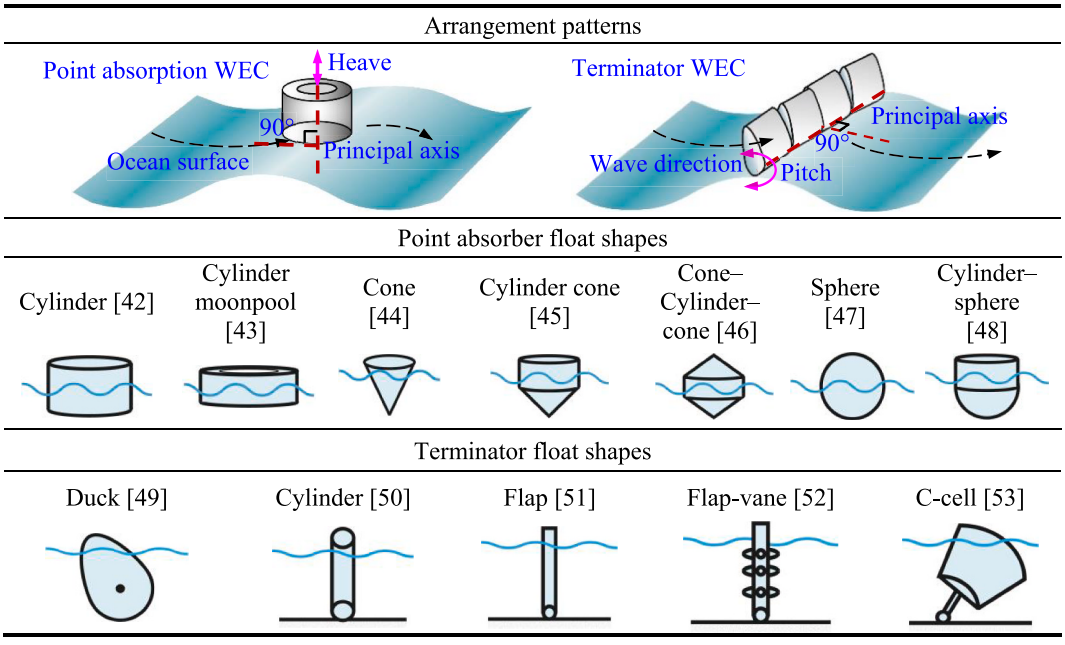

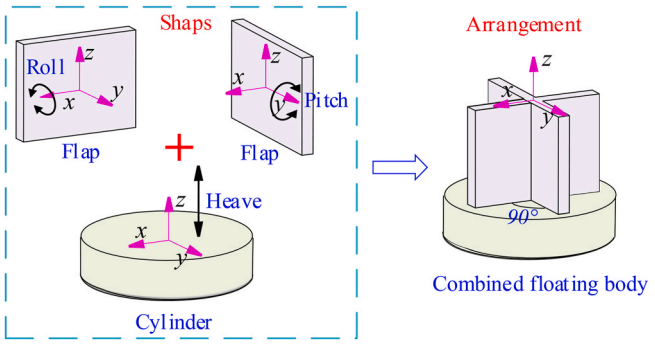

Fig. 2. Combined floating body of PCWEC.

As the relatively simple float structure facilitates the production and assembly of the actual prototype, the cylindrical and flap structures are selected to construct the PCWEC's floating body. Moreover, considering that the roll direction can be seen from the arrangement of the floating body as the equivalent of pitch, the two flaps are arranged in a 90-degree center symmetrical cross arrangement and combined with the cylinder to obtain the novel combined floating body (See Fig. 2). The designed floating body can successfully capture wave energy from the heave, pitch and roll motion, and its axisymmetric layout can reduce the cost of manufacturing, assembling and purchasing.

2.2. Limb design

The limbs connect the floating body and the fixed platform, and its structural characteristics determine the functions the PCWEC can achieve. At present, many mechanism synthesis approaches, such as displacement sub-group theory, graph theory, screw theory, linear translation, position and orientation characteristic set theory and GF set theory, can design the above limbs' structure [54]. Thereinto, GF theory [55] has practical, efficient and general performance and is better suited to design PCWEC's limbs.

Furthermore, the limbs of the parallel mechanism have active and passive types [56,57]. The active limb is an unconstrained branch that ensures the determinate motion of the end-effector, whereas the passive limb provides all necessary motion constraints to the end-effector and determines the DOF of the parallel mechanism. Thus, we select the active limb with three rotations and three translations (T_a T_b T_c; R_a R_b R_c) and the passive limb with two rotations and one translation (0 0 T_c; R_a R_b 0) to meet the combined floating body's freedom requirements. According to GF theory, we can quickly obtain the structure containing

Table 3
The limbs structure of PCWEC.

Simple kinematic pairs			
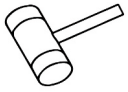 R	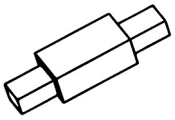 P	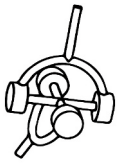 U	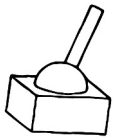 S
Passive limb structure with GF (0 0 0; R_a R_b 0) characteristic			
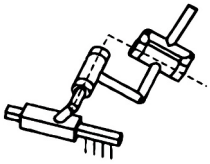 RP ($T_c \nparallel R_a$)	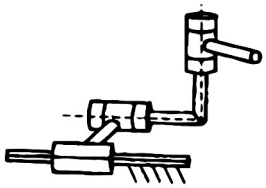 RP (T_c // R_a)	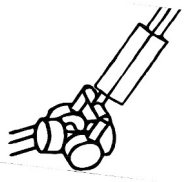 UP	
Active limb structure with GF (T_a T_b T_c; R_a R_b R_c) characteristic			
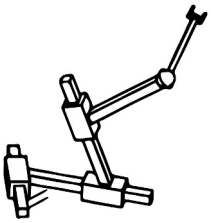 PPPS	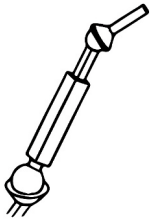 SPS	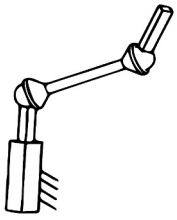 PSS	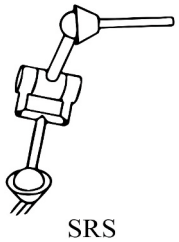 SRS
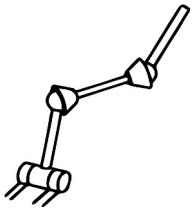 RSS	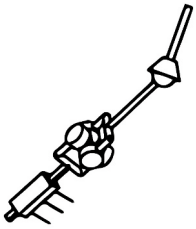 PUS	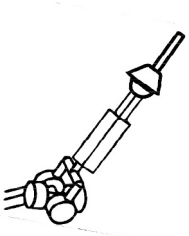 UPS	

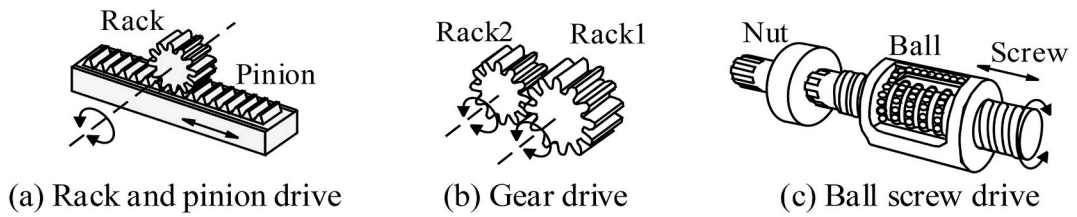

Fig. 3. The traditional mechanical transmission type PTO.

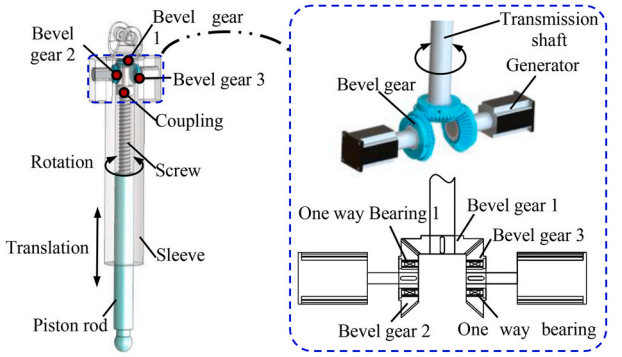

Fig. 4. Mobile self-rectifying PTO design.

the GF (T_a T_b T_c; R_a R_b R_c) characteristic active limb and GF (0 0 T_c; R_a R_b 0) characteristic passive limb (See Table 3). We only design the limbs composed of simple kinematic pairs, namely R (Rotation joint), U (Universal joint), P (Translation joint) and S (Sphere joint) and do not consider the limb structure composed of complex kinematic pairs to decrease the probability of failure and enhance the reliability of PCWEC.

Although the limb structure shown in Table 3 can satisfy the requirements of the designed floating body movement, the more kinematic pairs, the greater the probability of PCWEC damage in complex marine environments. Thus, selecting the UP structure as the passive limb of PCWEC is relatively reasonable. In addition, given that the spherical joint can bear more significant radial force and the universal joint has larger angles between shafts [58,59], connecting the spherical joint and the universal joint to the fixed platform and the floating body respectively can improve the PCWEC resistance to waves while increasing the workspace. Therefore, selecting the UPS structure as the active limb is more appropriate.

2.3. PTO design

As the last step of energy conversion of WEC, PTO converts valuable mechanical energy into electrical energy, which plays an essential role in power generation. The continuity and stability of power generation are critical issues for designing PTO. As shown in Fig. 3, the traditional mechanical transmission type PTO cannot output a fixed rotation direction because of the reciprocation of the rotation and movement of the PCWEC, which affect the service life of the generator and reduce the power generation efficiency after being directly transmitted to the generator. Furthermore, given that the designed active limb has UPS structure, translation joints for power generation are the only option. Thus, converting the reciprocating linear motion into the one-way rotation is essential for PCWEC's PTO design.

The one-way rotation characteristic of one-way bearings can address this problem at the level of mechanical transmission. Thus, to meet the requirements of power generation continuity and stability, we designed a mobile self-rectifying PTO based on one-way bearings and UPS active limbs. As shown in Fig. 4, when the piston push rod moves up relative to the sleeve, the transmission shaft turns clockwise by the ball screw drive (view from the top of Fig. 4b). According to the gear meshing relationship, the second bevel gear rotates counterclockwise (view from the left of Fig. 4b), and the third bevel gear rotates clockwise (view from the left of Fig. 4b). The first one-way bearing is idle and does not transmit torque, whereas the second one-way bearing rotates clockwise, which drives the right-side generator to work and generate current. Similarly, the first one-way bearing rotates clockwise when the transmission shaft moves down and drives the left side generator to generate current. Thus the PTO's output current direction remains unchanged no matter how the piston rod moves.

2.4. Configuration synthesis

The above studies have obtained structures including floating body, PTO and limbs. Combined with the basic overall structure of PCWEC shown in Fig. 1, we can obtain the PCWEC configuration using the axisymmetric installation method. Fig. 5 shows that the PCWEC comprises the combined floating body, four UPS power generation active

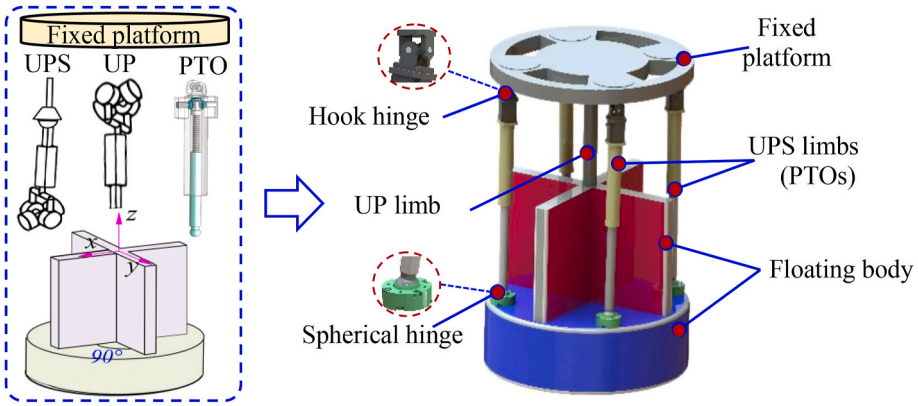

Fig. 5. The configuration synthesis of PCWEC.

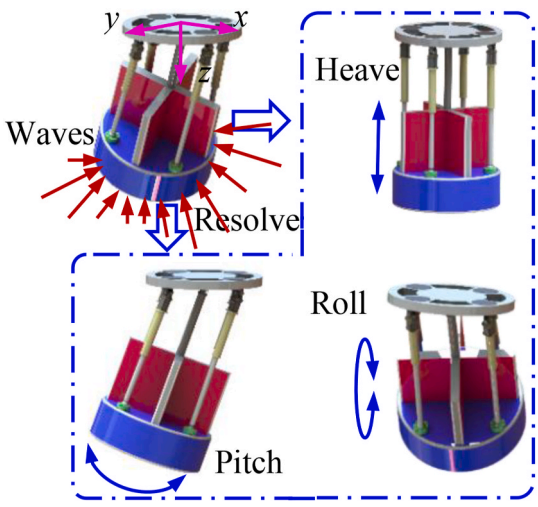

Fig. 6. The motion illustration of PCWEC.

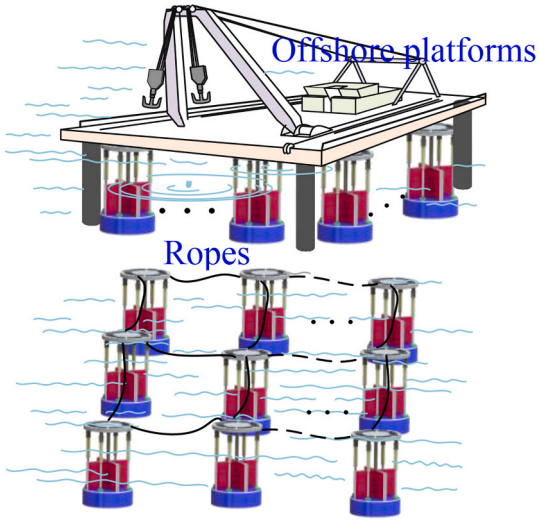

Fig. 7. The application scenarios of PCWEC.

limbs, a proper-constraint passive UP limb and a fixed platform. One end of the four active limbs is connected with the fixed platform through universal joints. The other end is connected with the combined floating body through sphere joints, showing axisymmetric distribution characteristics in space. One end of the passive limb is connected with the fixed platform through the universal joint, and the other end is connected with the combined floating body through the translation joint.

Excited by the irregularity of the waves, the designed PCWEC can realize the two-dimensional reciprocating rotation of pitch and surge and one-dimensional reciprocating movement of heave within a specific range (See Fig. 6), which conforms to the characteristics of wave motion and the sustainable power generation needs of the WEC. Moreover, the compact structure with multiple limbs arranged in a spatially balanced manner improves the stability of the WEC and brings flexible application scenarios to it. As shown in Fig. 7, PCWEC can be installed on fixed offshore platforms and float on the sea in groups through ropes. Such large-scale offshore power plants also facilitate the large-scale promotion of wave energy generation.

3. Energy conversion modeling

The reliability of PCWEC can be guaranteed with the proposed design in Section 2. This section takes irregular wave states into consideration and establishes the kinematic response model as well as the dynamic response model of PCWEC to evaluate the performance of the proposed PCWEC further.

3.1. Irregular wave model

Ocean waves are vibrations with random wave height, phase and periodic fluctuations. Therefore, the motion can be considered a combination of numerous disordered harmonic components in the design and analysis. As illustrated in Fig. 8, simple harmonic waves can represent irregular waves.

With the basic model given in Ref. [60], the irregular wave surface elevation can be described by Eq. (1)

$$\eta(x,t)=\sum_{i=1}^{\infty}\frac{H_i}{2}\cos\left(\frac{2\pi}{T_i}t-\frac{2\pi}{L_i}x+\varepsilon_i\right) \tag{1}$$

where H_i, T_i, L_i, and ε_i represent the height, period, wavelength, and phase of irregular waves, respectively. X and t are the position and time of wave motion, respectively.

The Joint North Sea Wave Project (JONSWAP) spectrum is consistent with the measured results of waves [61] and applies to waveforms in different growth stages. Thus, the JONSWAP wave spectrum function is adopted to describe the irregular wave height, as given by Eq. (2)

$$H=2\sqrt{2S(\omega_n)\Delta\omega_n} \tag{2}$$

where ω_n and $\Delta\omega_n$ are the wave excitation frequency and frequency bandwidth, respectively. $S(\omega_n)$ represents JONSWAP wave spectrum, and is given as follows

$$S(\omega_n)=\frac{\alpha g^2}{\omega_n^5}\exp\left[-1.25\left(\frac{\omega_m}{\omega_n}\right)^4\right]\gamma^{\exp\left[-(\omega_n-\omega_m)^2/\left(2\sigma^2\omega_m^2\right)\right]} \tag{3}$$

$$\alpha=5.061\left(\frac{\omega_m}{2\pi}\right)^4H_{1/3}^2(1-0.287\log\gamma) \tag{4}$$

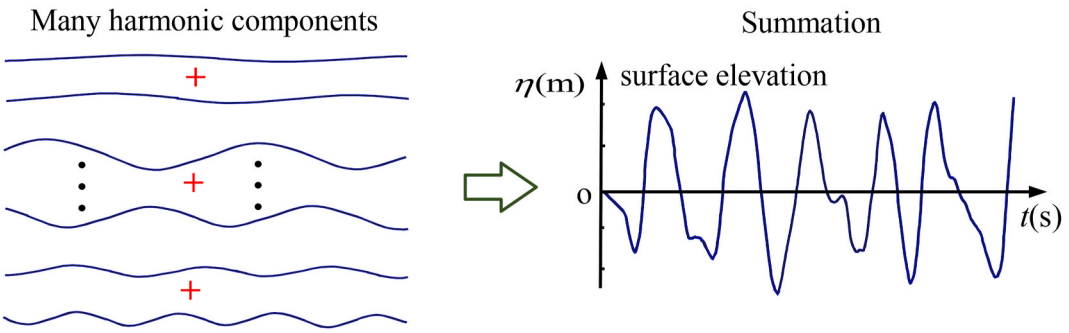

Fig. 8. Irregular wave generation schematic.

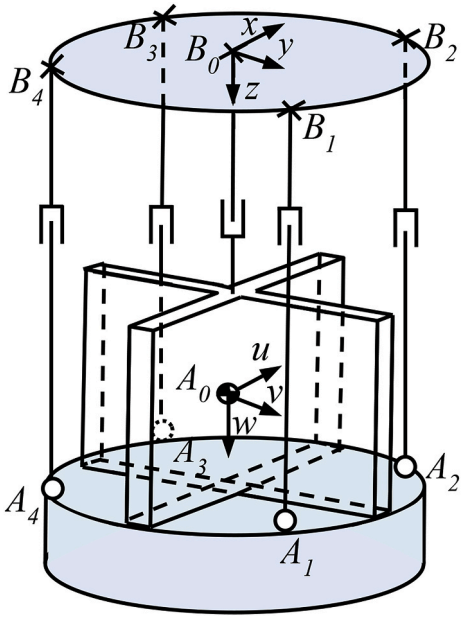

Fig. 9. Structure sketch of PCWEC.

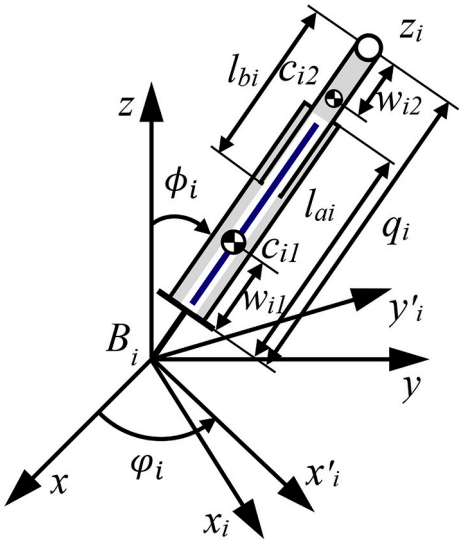

Fig. 10. The local coordinate system of the *i*th limb.

where g and $H_{1/3}$ are the acceleration of gravity and significant wave height, respectively. γ is peak enhancement parameter, and ω_m is the peak frequency. In general, $\sigma \approx 0.07$ for $\omega_n \leq \omega_m$; otherwise, $\sigma \approx 0.09$ for $\omega_n > \omega_m$ [61].

3.2. Kinematic response model

3.2.1. Coordinate system

As shown in Fig. 9, the coordinate system of the PCWEC is established. The $B_0 - xyz$ is a reference coordinate system, where the x-axis points from B_0 to the midpoint of the line connecting B_2 and B_3, the z-axis is vertical to the fixed platform downward, and the y-axis satisfies the right-hand rule. The moving coordinate system $A_0 - uvw$ is established with the mass center A_0 of the floating body as the reference point. The u-axis points from the A_0 point to the midpoint of the line connecting A_2 and A_3. The w-axis goes down along the axisymmetric central axis of the combined floating body, and the v-axis direction satisfies the right-hand rule.

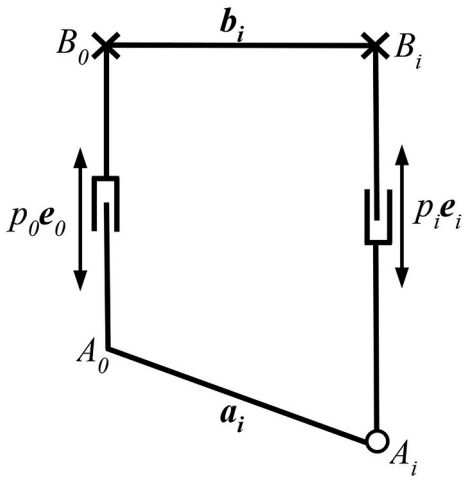

Fig. 11. Vector diagram of the *i*th limb.

The orientation of the floating body can be described by the rotation matrix ${}^{B0}\boldsymbol{R}_{A0}$, as given in Eq. (5).

$$ {}^{B0}\boldsymbol{R}_{A0} = \boldsymbol{R}_{rot(y)}(\psi_y)\boldsymbol{R}_{rot(x)}(\psi_x) = \begin{bmatrix} \cos\psi_y & \sin\psi_y \sin\psi_y & \cos\psi_x \sin\psi_y \\ 0 & \cos\psi_x & -\sin\psi_x \\ -\sin\psi_y & \cos\psi_y \sin\psi_x & \cos\psi_x \cos\psi_y \end{bmatrix} \tag{5} $$

where ψ_x, ψ_y and ψ_z are the Euler angles of the floating body rotating around x, y and z, respectively.

To describe the orientation of each limb, the local coordinate system $B_i - x_i y_i z_i$ is established, as shown in Fig. 10. Two Euler angles φ_i and φ_i are used to represent the orientation relationship between the $B_0 - xyz$ and the $B_i - x_i y_i z_i$. Therefore, the rotation matrix ${}^{B0}\boldsymbol{R}_{Bi}$ can be defined as follows

$$ {}^{B_0}\boldsymbol{R}_{Bi} = \boldsymbol{R}_{rot(z)}(\varphi_i)\boldsymbol{R}_{rot(y)}(\varphi_i) = \begin{bmatrix} \cos\varphi_i \cos\varphi_i & -\sin\varphi_i & \cos\varphi_i \sin\varphi_i \\ \sin\varphi_i \cos\varphi_i & \cos\varphi_i & \sin\varphi_i \sin\varphi_i \\ -\sin\varphi_i & 0 & \cos\varphi_i \end{bmatrix} \tag{6} $$

3.2.2. Position analysis

With the vector diagram of the *i*th limb shown in Fig. 11, the position equation associated with the *i*th limb can be described by

$$ p_0\boldsymbol{e}_0 + \boldsymbol{a}_i = \boldsymbol{b}_i + p_i\boldsymbol{e}_i \tag{7} $$

where p_0, p_i, $\boldsymbol{e}_0$, $\boldsymbol{e}_i$, $\boldsymbol{a}_i$ and $\boldsymbol{b}_i$ represent the length of the central passive limb, the length of the *i*th active limb, the unit vector along the central passive limb, the vector along the *i*th active limb, the vector $\overrightarrow{A_0A_i}$, and the vector $\overrightarrow{B_0B_i}$, respectively.

With Eq. (7), the length of active limb can be derived as

$$ p_i = \sqrt{(p_0\boldsymbol{e}_0 + \boldsymbol{a}_i - \boldsymbol{b}_i)^T(p_0\boldsymbol{e}_0 + \boldsymbol{a}_i - \boldsymbol{b}_i)} \tag{8} $$

3.2.3. Velocity analysis

Taking the derivative of Eq. (7) on both sides with respect to the time, we have

$$ \boldsymbol{v} + \boldsymbol{\omega} \times \boldsymbol{a}_i = \dot{p}_i\boldsymbol{e}_i + \boldsymbol{\omega}_i \times p_i\boldsymbol{e}_i \tag{9} $$

where $\boldsymbol{\omega}_i$ denotes the angular velocity of *i*th active limb, $\boldsymbol{v}$ and $\boldsymbol{\omega}$ represent the floating body's linear and angular velocity.

Taking the dot product of both sides of Eq. (9) with $\boldsymbol{e}_i$, the linear velocity of the *i*th active limb in matrix form is given by

$$ \dot{\boldsymbol{p}} = [\dot{p}_1 \quad \dot{p}_2 \quad \dot{p}_3 \quad \dot{p}_4]^T = \boldsymbol{J}\dot{\boldsymbol{X}} = \boldsymbol{J}\begin{bmatrix} \boldsymbol{v} \\ \boldsymbol{\omega} \end{bmatrix} \tag{10} $$

where

$$\boldsymbol{J}=\begin{bmatrix} \boldsymbol{e}_1 & \boldsymbol{e}_2 & \boldsymbol{e}_3 & \boldsymbol{e}_4 \\ (\boldsymbol{a}_1\times\boldsymbol{e}_1) & (\boldsymbol{a}_2\times\boldsymbol{e}_2) & (\boldsymbol{a}_3\times\boldsymbol{e}_3) & (\boldsymbol{a}_4\times\boldsymbol{e}_4) \end{bmatrix}^T \tag{11}$$

Taking the derivative of left side of equation (7) with respect to time, we get the velocity of the point of the A_i

$$\boldsymbol{v}_{Ai}=\boldsymbol{v}+\boldsymbol{\omega}\times\boldsymbol{a}_i \tag{12}$$

The right sides of Eq. (7) is derived for time t, and we have

$$\boldsymbol{v}_{A_i}=\dot{p}_i\boldsymbol{e}_i+\boldsymbol{\omega}_i\times p_i\boldsymbol{e}_i \tag{13}$$

Taking the cross product of both sides of Eq. (13) with $\boldsymbol{e}_i$ and combine with Eq. (12), we can get

$$\boldsymbol{\omega}_i=\frac{1}{p_i}\boldsymbol{S}(\boldsymbol{e}_i)(\boldsymbol{v}+\boldsymbol{S}(\boldsymbol{\omega})\boldsymbol{a}_i) \tag{14}$$

where $\boldsymbol{S}(\cdot)$ is the screw matrix.

Describe Eq. (14) in the coordinate system $B_i-x_iy_iz_i$.

$$\begin{aligned}{}^{B_i}\boldsymbol{\omega}_i&=\frac{1}{p_i}\begin{bmatrix}\boldsymbol{S}({}^{B_i}\boldsymbol{e}_i){}^{B_i}\boldsymbol{R}_{B_0} & -\boldsymbol{S}({}^{B_i}\boldsymbol{e}_i)\boldsymbol{S}({}^{B_i}\boldsymbol{a}_i){}^{B_i}\boldsymbol{R}_{B_0}\end{bmatrix}\begin{bmatrix}\boldsymbol{v}\\ \boldsymbol{\omega}\end{bmatrix}\\ &=\boldsymbol{J}_{i\omega}\begin{bmatrix}\boldsymbol{v}\\ \boldsymbol{\omega}\end{bmatrix}\quad i=1,2,3,4\end{aligned} \tag{15}$$

$${}^{B_0}\boldsymbol{\omega}_0=\begin{bmatrix}\boldsymbol{0}_{3\times3} & \boldsymbol{E}_{3\times3}\end{bmatrix}\begin{bmatrix}\boldsymbol{v}\\ \boldsymbol{\omega}\end{bmatrix}=\boldsymbol{J}_{0\omega}\dot{\boldsymbol{X}}=\boldsymbol{\omega} \tag{16}$$

In the coordinate system $B_i-x_iy_iz_i$, the linear velocity of the mass center c_{i1} in the ith sleeve is expressed by

$${}^{B_i}\boldsymbol{v}_{ci1}=\left(w_{i1}{}^{B_i}\boldsymbol{e}_i\right)\times{}^{B_i}\boldsymbol{\omega}_i \tag{17}$$

Substitute Eq. (15) into Eq. (17) to obtain

$${}^{B_i}\boldsymbol{v}_{ci1}=-\boldsymbol{S}\left(w_{i1}{}^{B_i}\boldsymbol{e}_i\right)\boldsymbol{J}_{i\omega}\begin{bmatrix}\boldsymbol{v}\\ \boldsymbol{\omega}\end{bmatrix}=\boldsymbol{J}_{vci1}\dot{\boldsymbol{X}} \tag{18}$$

In the coordinate system $B_i-x_iy_iz_i$, the linear velocity of the mass center c_{i2} in the ith piston rod is described by

$${}^{B_i}\boldsymbol{v}_{ci2}={}^{B_i}\boldsymbol{v}+{}^{B_i}\boldsymbol{\omega}\times{}^{B_i}\boldsymbol{a}_i-{}^{B_i}\boldsymbol{\omega}_i\times\left(w_{i2}{}^{B_i}\boldsymbol{e}_i\right) \tag{19}$$

Substitute Eq. (15) into Eq. (19) to get

$${}^{B_i}\boldsymbol{v}_{c_{i2}}=\left(\begin{bmatrix}{}^{B_i}\boldsymbol{R}_{B_0} & -\boldsymbol{S}({}^{B_i}\boldsymbol{a}_i){}^{B_i}\boldsymbol{R}_{B_0}\end{bmatrix}+\boldsymbol{S}\left(w_{i2}{}^{B_i}\boldsymbol{e}_i\right)\boldsymbol{J}_{i\omega}\right)\begin{bmatrix}\boldsymbol{v}\\ \boldsymbol{\omega}\end{bmatrix} \tag{20}$$

where

$$\boldsymbol{J}_{vc_{i2}}=\begin{bmatrix}{}^{B_i}\boldsymbol{R}_{B_0} & -\boldsymbol{S}({}^{B_i}\boldsymbol{a}_i){}^{B_i}\boldsymbol{R}_{B_0}\end{bmatrix}+\boldsymbol{S}\left(w_{i2}{}^{B_i}\boldsymbol{e}_i\right)\boldsymbol{J}_{i\omega}\quad i=1,2,3,4 \tag{21}$$

The velocity of the central passive limb piston rod is as follows

$${}^{B_0}\boldsymbol{v}_{c02}=\boldsymbol{\omega}\times\left(w_{02}\boldsymbol{e}_0\right) \tag{22}$$

3.2.4. Acceleration analysis

Taking the time derivative of Eq. (7) and taking both sides dot product with $\boldsymbol{w}_i$ of the equation, and then writing it in the matrix form, we can establish the acceleration mapping relationship between the floating body and the active limb.

$$\ddot{\boldsymbol{q}}=\boldsymbol{J}\begin{bmatrix}\dot{\boldsymbol{v}}\\ \dot{\boldsymbol{\omega}}\end{bmatrix}+\begin{bmatrix}p_1\left(\boldsymbol{\omega}_1^T\boldsymbol{\omega}_1\right)+\left(\boldsymbol{e}_1^T\boldsymbol{\omega}\right)\left(\boldsymbol{\omega}^T\boldsymbol{a}_1\right)-\left(\boldsymbol{e}_1^T\boldsymbol{a}_1\right)\left(\boldsymbol{\omega}^T\boldsymbol{\omega}\right)\\ p_2\left(\boldsymbol{\omega}_2^T\boldsymbol{\omega}_2\right)+\left(\boldsymbol{e}_2^T\boldsymbol{\omega}\right)\left(\boldsymbol{\omega}^T\boldsymbol{a}_2\right)-\left(\boldsymbol{e}_2^T\boldsymbol{a}_2\right)\left(\boldsymbol{\omega}^T\boldsymbol{\omega}\right)\\ p_3\left(\boldsymbol{\omega}_3^T\boldsymbol{\omega}_3\right)+\left(\boldsymbol{e}_3^T\boldsymbol{\omega}\right)\left(\boldsymbol{\omega}^T\boldsymbol{a}_3\right)-\left(\boldsymbol{e}_3^T\boldsymbol{a}_3\right)\left(\boldsymbol{\omega}^T\boldsymbol{\omega}\right)\\ p_4\left(\boldsymbol{\omega}_4^T\boldsymbol{\omega}_4\right)+\left(\boldsymbol{e}_4^T\boldsymbol{\omega}\right)\left(\boldsymbol{\omega}^T\boldsymbol{a}_4\right)-\left(\boldsymbol{e}_4^T\boldsymbol{a}_4\right)\left(\boldsymbol{\omega}^T\boldsymbol{\omega}\right)\end{bmatrix} \tag{23}$$

Taking the derivative of the right side of Eq. (13) concerning time and taking the cross product of both sides for the equation with ${}^{B_i}\boldsymbol{w}_i$, the angular acceleration in the coordinate system $B_i-x_iy_iz_i$ of the ith active limb can be described as follows:

$${}^{B_i}\dot{\boldsymbol{\omega}}_i=\boldsymbol{J}_{i\omega}\begin{bmatrix}\dot{\boldsymbol{v}}\\ \dot{\boldsymbol{\omega}}\end{bmatrix}+\frac{1}{p_i}\begin{pmatrix}\left({}^{B_i}\boldsymbol{\omega}^{TB_i}\boldsymbol{a}_i\right)\left({}^{B_i}\boldsymbol{e}_i\times{}^{B_i}\boldsymbol{\omega}\right)\\ -\left({}^{B_i}\boldsymbol{\omega}^{TB_i}\boldsymbol{\omega}\right)\left({}^{B_i}\boldsymbol{e}_i\times{}^{B_i}\boldsymbol{a}_i\right)-2\dot{p}_i{}^{B_i}\boldsymbol{\omega}_i\end{pmatrix} \tag{24}$$

Since the angular acceleration of the passive limb is equal to that of the floating body, we can have

$${}^{B_0}\dot{\boldsymbol{\omega}}_0=\boldsymbol{J}_{0\omega}\begin{bmatrix}\dot{\boldsymbol{v}}\\ \dot{\boldsymbol{\omega}}\end{bmatrix}=\boldsymbol{\omega} \tag{25}$$

Taking the derivative of both ends of Eq. (17) concerning time and substituting Eq. (24) into it, we can obtain the linear acceleration of the mass center c_{i1} for the ith sleeve in the coordinate system $B_i-x_iy_iz_i$.

$$\begin{aligned}{}^{B_i}\dot{\boldsymbol{v}}_{c_{i1}}=\boldsymbol{J}_{vc_{i1}}\begin{bmatrix}\dot{\boldsymbol{v}}\\ \dot{\boldsymbol{\omega}}\end{bmatrix}-\frac{1}{q_i}\Bigg(&\left(\left({}^{B_i}\boldsymbol{\omega}^{TB_i}\boldsymbol{a}_i\right)\left({}^{B_i}\boldsymbol{w}_{i1}^{TB_i}\boldsymbol{\omega}\right)-\left({}^{B_i}\boldsymbol{\omega}^{TB_i}\boldsymbol{\omega}\right)\left({}^{B_i}\boldsymbol{w}_{i1}^{TB_i}\boldsymbol{a}_i\right)\right){}^{B_i}\boldsymbol{e}_i\\ &+w_{i1}\left(-\left({}^{B_i}\boldsymbol{\omega}^{TB_i}\boldsymbol{a}_i\right){}^{B_i}\boldsymbol{\omega}+\left({}^{B_i}\boldsymbol{\omega}^{TB_i}\boldsymbol{\omega}\right){}^{B_i}\boldsymbol{a}_i\right)\\ &+2\dot{p}_i\left({}^{B_i}\boldsymbol{\omega}_i\times{}^{B_i}\boldsymbol{w}_{i1}\right)\\ &-\left({}^{B_i}\boldsymbol{\omega}_i^{TB_i}\boldsymbol{\omega}_i\right){}^{Bi}\boldsymbol{w}_{i1}\quad i=1,2,3,4\Bigg)\end{aligned} \tag{26}$$

Taking the derivative of both ends of Eq. (20) concerning time and substituting Eq. (24) into it, we can obtain the linear acceleration of the mass center c_{i2} for the ith piston rod in the coordinate system $B_i-x_iy_iz_i$.

$$\begin{aligned}{}^{B_i}\dot{\boldsymbol{v}}_{c_{i2}}=&\boldsymbol{J}_{vc_{i2}}\begin{bmatrix}\dot{\boldsymbol{v}}\\ \dot{\boldsymbol{\omega}}\end{bmatrix}+{}^{B_i}\boldsymbol{\omega}\times\left({}^{B_i}\boldsymbol{\omega}\times{}^{B_i}\boldsymbol{a}_i\right)-{}^{B_i}\boldsymbol{\omega}_i\times\left({}^{B_i}\boldsymbol{\omega}_i\times{}^{B_i}\boldsymbol{w}_{i2}\right)\\ &+\frac{1}{p_i}S\left({}^{B_i}\boldsymbol{w}_{i2}\right)\begin{pmatrix}\left({}^{B_i}\boldsymbol{\omega}^{TB_i}\boldsymbol{a}_i\right)\left({}^{B_i}\boldsymbol{e}_i\times{}^{B_i}\boldsymbol{\omega}\right)\\ -\left({}^{B_i}\boldsymbol{\omega}^{TB_i}\boldsymbol{\omega}\right)\left({}^{B_i}\boldsymbol{e}_i\times{}^{B_i}\boldsymbol{a}_i\right)-2\dot{p}_i{}^{B_i}\boldsymbol{\omega}_i\end{pmatrix}\end{aligned} \tag{27}$$

Taking the derivative of Eq. (22) concerning time, we can get the acceleration of the central passive limb piston rod as follows

$${}^{B_0}\dot{\boldsymbol{v}}_{c02}=\dot{\boldsymbol{\omega}}\times\boldsymbol{w}_{02}+\boldsymbol{\omega}\times(\boldsymbol{\omega}\times\boldsymbol{w}_{02}) \tag{28}$$

3.3. Dynamic response model

3.3.1. Force analysis

The floating body relies on hydrostatic buoyancy to maintain balance and remain stationary in the calm ocean. When there are waves, the floating body is subjected to irregular motion by the ocean wave force, which makes the PTO connected to it generate electricity. Under the action of the wave, the wave force and moment of the floating body are as follows

$$\boldsymbol{F}_d(t)=\boldsymbol{F}_{res}(t)+\boldsymbol{F}_{ext}(t)+\boldsymbol{F}_{rad}(t) \tag{29}$$

$$\boldsymbol{M}_d(t)=\boldsymbol{M}_{res}(t)+\boldsymbol{M}_{ext}(t)+\boldsymbol{M}_{rad}(t) \tag{30}$$

where $\boldsymbol{F}_{ext}$, $\boldsymbol{F}_{hs}$ and $\boldsymbol{F}_{rad}$ represent the wave excitation force, hydrostatic buoyancy and radiation damping force received by the floating body in ocean waves, respectively. $\boldsymbol{M}_{ext}$, $\boldsymbol{M}_{hs}$ and $\boldsymbol{M}_{rad}$ represent the moments produced by these three wave forces, respectively. According to the hydrostatic force equation [62] and Cummins equation [63], they are expressed as follows

$$\boldsymbol{F}_{hs}(t)=\rho\boldsymbol{g}V_0\ ,\quad \boldsymbol{M}_{hs}=\boldsymbol{F}_{hs}(t)\times(q_0\boldsymbol{w}_0) \tag{31}$$

$$\boldsymbol{F}_{ext}=\int_{-\infty}^{\infty}\boldsymbol{IRF}_{ext}(t-\tau)\eta(\tau)d\tau,\boldsymbol{M}_{ext}=\boldsymbol{F}_{ext}(t)\times(q_0\boldsymbol{w}_0) \tag{32}$$

$$\boldsymbol{F}_{rad}=-\boldsymbol{m}_{add,\infty}\ddot{\boldsymbol{X}}-\int_0^t\boldsymbol{IRF}_{rad}(t-\tau)\ddot{\boldsymbol{X}}(\tau)d\tau,\boldsymbol{M}_{rad}=\boldsymbol{F}_{rad}(t)\times(q_0\boldsymbol{w}_0) \tag{33}$$

where ρ, $\boldsymbol{g}$, V_0 respectively represent seawater density, gravitational acceleration, and volume of the fluid displaced by the floating body.

$\boldsymbol{IRF}_{ext}$, $\boldsymbol{IRF}_{rad}$ and $\boldsymbol{m}_{add,\infty}$ denote impulse response function of excitation wave, impulse response function of radiation wave, and additional mass coefficient, respectively.

We can obtain the resultant force/moment acting on the mass center of the floating body by using Newton's Euler equations.

$$\boldsymbol{H}=\begin{bmatrix}\boldsymbol{f}\\ \boldsymbol{n}\end{bmatrix}=\begin{bmatrix}(\boldsymbol{F}_d+m\boldsymbol{g}-m\dot{\boldsymbol{v}})\\ \boldsymbol{M}_d-{}^{B_0}\boldsymbol{I}\dot{\boldsymbol{\omega}}-\boldsymbol{\omega}\times\left({}^{B_0}\boldsymbol{I}\boldsymbol{\omega}\right)\end{bmatrix} \tag{34}$$

where m and ${}^{B_0}\boldsymbol{I}$ represent the mass of the floating body and the inertia matrix of the floating body in the coordinate system $B_i-\ x_iy_iz_i$, respectively.

The following equation is the resultant force/moment exerted on the mass centers c_{i1} and c_{i2}:

$${}^{B_i}\boldsymbol{H}_{c_{i1}}=\begin{bmatrix}{}^{B_i}\boldsymbol{f}_{c_{i1}}\\ {}^{B_i}\boldsymbol{n}_{c_{i1}}\end{bmatrix}=\begin{bmatrix}m_{c_{i1}}{}^{B_i}\boldsymbol{R}_{B_0}\boldsymbol{g}-m_{c_{i1}}\dot{\boldsymbol{v}}_{c_{i1}}\\ -{}^{B_i}\boldsymbol{I}_{c_{i1}}\dot{\boldsymbol{\omega}}_i-{}^{B_i}\boldsymbol{\omega}_i\times\left({}^{B_i}\boldsymbol{I}_{c_{i1}}{}^{B_i}\boldsymbol{\omega}_i\right)\end{bmatrix} \tag{35}$$

$${}^{B_i}\boldsymbol{H}_{c_{i2}}=\begin{bmatrix}{}^{B_i}\boldsymbol{f}_{c_{i2}}\\ {}^{B_i}\boldsymbol{n}_{c_{i2}}\end{bmatrix}=\begin{bmatrix}m_{c_{i2}}{}^{B_i}\boldsymbol{R}_{B_0}\boldsymbol{g}-m_{c_{i2}}\dot{\boldsymbol{v}}_{c_{i2}}\\ -{}^{B_i}\boldsymbol{I}_{c_{i2}}\dot{\boldsymbol{\omega}}_i-{}^{B_i}\boldsymbol{\omega}_i\times\left({}^{B_i}\boldsymbol{I}_{c_{i2}}{}^{B_i}\boldsymbol{\omega}_i\right)\end{bmatrix} \tag{36}$$

where m_{ci1}, m_{ci2}, ${}^{B_i}\boldsymbol{I}_{ci1}$, and ${}^{B_i}\boldsymbol{I}_{ci2}$ represent the sleeve's mass, piston rod's mass of the ith active limb, the sleeve's inertia matrix, and the piston rod's inertia matrix of the ith active limb in the coordinate system $B_i-\ x_iy_iz_i$, respectively.

In the power conversion process of the PTO, the ball screw, coupling, bevel gear and generator rotor only contain rotation. Therefore, the resultant of applied and inertia forces exerted on the PTO can be obtained

$$\boldsymbol{N}_i=\left(F_{bi}-[I_{Si}+I_{Ci}+I_{Bi}+I_{Mi})]\ddot{\theta}_{SCi}\right){}^{B_i}\boldsymbol{e}_i \tag{37}$$

where I_{Si}, I_{Ci}, I_{Bi}, and I_{Mi} represent the rotational inertia of the ith ball screw, coupling, bevel gear set, and generator rotor, respectively. F_{bi} and $\ddot{\theta}_{SCi}$ denote the axial dynamic response force and angular acceleration of the ith ball screw.

The kinematic relationship between the piston rod and ball screw is as follows

$$\ddot{\theta}_{SCi}=\frac{2\pi}{Ph}\ddot{p}_i \tag{38}$$

where Ph represents the lead of the ball screw.

According to the principle of virtual work, the sum of virtual work done by applied and inertia forces exerted overall PCWEC is zero, and hence we can have

$$\delta\boldsymbol{X}^T\boldsymbol{H}+\sum_{i=1}^{4}\left(\delta\boldsymbol{X}_{c_{i1}}^T\boldsymbol{H}_{c_{i1}}\right)+\sum_{i=0}^{4}\left(\delta\boldsymbol{X}_{c_{i2}}^T\boldsymbol{H}_{c_{i2}}\right)+\delta\boldsymbol{\theta}^T\boldsymbol{N}=0 \tag{39}$$

where

$$\delta\boldsymbol{X}_{c_{i1}}=[\boldsymbol{J}_{vc_{i1}}\quad\boldsymbol{J}_{i\omega}]^T\delta\boldsymbol{X}=\boldsymbol{J}_{c_{i1}}\delta\boldsymbol{X} \tag{40}$$

$$\boldsymbol{N}=[\boldsymbol{N}_1\quad\boldsymbol{N}_2\quad\boldsymbol{N}_3\quad\boldsymbol{N}_4]^T \tag{41}$$

$$\delta\boldsymbol{X}_{c_{i2}}=[\boldsymbol{J}_{vc_{i2}}\quad\boldsymbol{J}_{i\omega}]^T\delta\boldsymbol{X}=\boldsymbol{J}_{c_{i2}}\delta\boldsymbol{X} \tag{42}$$

$$\delta\boldsymbol{\theta}=\mathrm{diag}\left(\frac{2\pi}{Ph_1},\frac{2\pi}{Ph_2},\frac{2\pi}{Ph_3},\frac{2\pi}{Ph_4}\right)\boldsymbol{J}\delta\boldsymbol{X}=\boldsymbol{A}\boldsymbol{J}\delta\boldsymbol{X} \tag{43}$$

where $\delta\boldsymbol{\theta}$ denotes the virtual rotation angle matrix of each PTO. $\delta\boldsymbol{X}$, $\delta\boldsymbol{X}_{ci1}$, and $\delta\boldsymbol{X}_{ci2}$ represent the matrix of virtual displacement and rotation angle for floating body's mass center A_0, sleeve's mass center c_{i1}, and piston rod's mass center c_{i2}.

Substitute Eqs. ((37) and (37) and (38) and (40)–(43) into Eq. (39), we can get

$$\boldsymbol{F}_b=-\boldsymbol{A}^{-T}\boldsymbol{J}^{-T}\left(\boldsymbol{H}+\sum_{i=1}^{4}\left(\boldsymbol{J}_{c_{i1}}^T{}^{B_i}\boldsymbol{H}_{c_{i1}}\right)+\sum_{i=0}^{4}\left(\boldsymbol{J}_{c_{i2}}^T{}^{B_i}\boldsymbol{H}_{c_{i2}}\right)\right)+\boldsymbol{I}_{SBCM}\boldsymbol{A}\ddot{\boldsymbol{p}} \tag{44}$$

where

$$\begin{aligned}&\boldsymbol{I}_{SCBM}=\mathrm{diag}(I_{SCBM1},I_{SCBM2},I_{SCBM3},I_{SCBM4})\\ &I_{SCBMi}=I_{Si}+I_{Ci}+I_{Bi}+I_{Mi}\end{aligned} \tag{45}$$

3.3.2. Power output analysis

Under wave force, the floating body drives the PTO to convert wave energy into electricity. In this process, the generator's output power can be obtained by analyzing its rotational speed and torque.

As from the schematic diagram of PTO in Fig. 4, the excitation torque converted to the input shaft of the generator can be expressed as follows

$$\tau_{Ti}=\frac{\lambda Ph}{2\pi}F_{bi}(i=1,2,3,4) \tag{46}$$

where τ_{Ti} represents the torque converted to the input shaft of the ith generator, λ denotes the transmission efficiency of the PTO.

The torque of the rotating generator is expressed as follows

$$\tau_{emi}=\tau_{Ti}-I_{Mi}\ddot{\theta}_{mi}=C_{pto}\dot{\theta}_{mi} \tag{47}$$

where τ_{emi}, $\dot{\theta}_{mi}$, $\dot{\theta}_{mi}$ and C_{pto} denote the torque, angular velocity, angular acceleration and damping coefficient of the ith active limb generator, respectively.

The instantaneous output power of each power generation active limb is

$$P_i=\tau_{emi}\dot{\theta}_{mi} \tag{48}$$

The generator speed direction of the designed mobile self-rectifying PTO is constant and always opposite to the direction of electromagnetic torque, where the generator's output power is specified to be positive. Thus, the absolute value should be taken in the numerical calculation of the output power, i. e

$$P=\sum_{i=1}^{4}\int_{t_0}^{t_f}|\tau_{emi}\dot{\theta}_{mi}|dt \tag{49}$$

where t_0 and t_f represent the initial operation time and the end time of the generator, respectively.

3.3.3. Energy cost-efficiency analysis

Commercial development experience would indicate that grabbing a more significant profit with a minimal investment cost is the most critical consideration in developing viable industrial equipment. This principle also applies to the development of WEC. Following this idea, we can define energy cost-efficiency to evaluate the commercial development potential of different OBWECs by integrating OBWEC's investment cost and power generation efficiency.

(1) Investment cost

The investment cost of OBWEC includes the cost of manufacturing, installation, maintenance, and power transmission and transformation operation. However, these detailed economic cost parameters are relatively scarce because wave power generation technology is not yet fully mature, and successful commercial development has few cases. Therefore, quantitatively calculating the investment costs of the OBWECs is quite challenging.

Historically, the cost of using sizeable mechanical equipment is directly proportional to the scale of the device, which is commonly known to the industry. Thus, using the scale Q of the OBWEC is acceptable to approximate the corresponding investment costs, especially in the conceptual design stage where many detailed economic cost

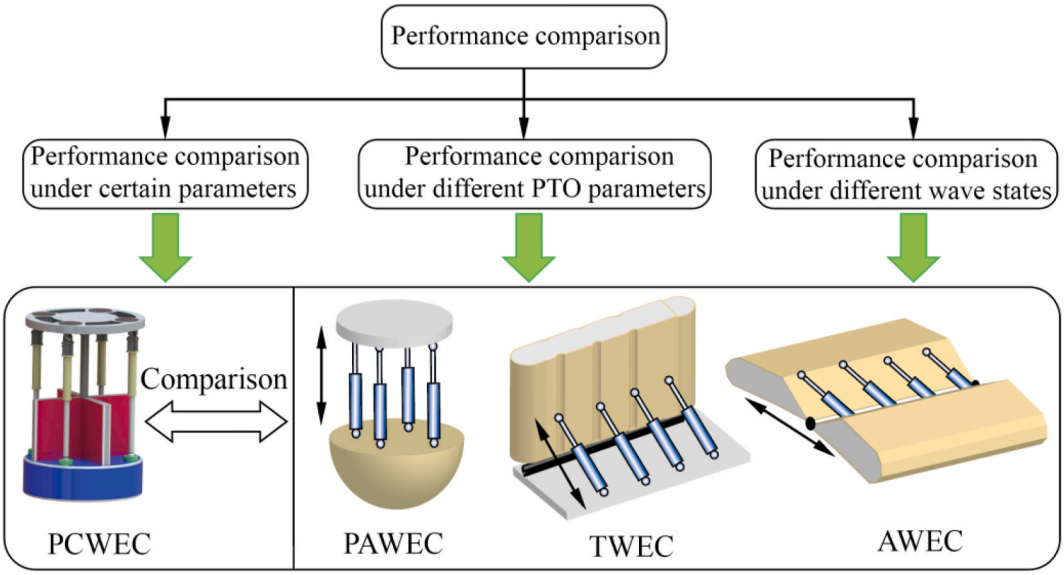

Fig. 12. Case description for performance comparison of the PCWEC.

Table 4
Dimensions and structural parameters of PCWEC.

Point coordinates of floating body (m)	A_0	A_1	A_2	A_3	A_4
	0.0000	1.7675	−1.7675	1.7675	−1.7675
	0.0000	1.7675	1.7675	−1.7675	−1.7675
	2.4500	3.0000	3.0000	3.0000	3.0000
Point coordinates of fixed platform (m)	B_0	B_1	B_2	B_3	B_4
	0.0000	1.7675	−1.7675	1.7675	1.7675
	0.0000	1.7675	1.7675	−1.7675	−1.7675
	0.0000	0.0000	0.0000	0.0000	0.0000
PCWEC Components	Parameters	Float body	Sleeve		Piston rod
	Mass (kg)	76.260	20.206		12.328
	Inertia tensor (kg·m^2)	$\mathrm{diag}\begin{pmatrix}68.717\\75.104\\68.717\end{pmatrix}$	$\mathrm{diag}\begin{pmatrix}4.855\\4.858\\0.168\end{pmatrix}$		$\mathrm{diag}\begin{pmatrix}5.821\\3.043\\5.821\end{pmatrix}$
PTO Components	Parameters	Ball screw	Coupling	Bevel gear set	Generator rotor
	Moment of inertia (kg·m^2)	20.6783	10.6524	12.2564	10.1528

Table 5
Characteristic parameters of offshore wave motion in the northern South China coast [65].

Significant wave height	Wave period	Wave direction	Peak enhancement parameter	Density
2.0m	8s	$\pi/6$	3.3	1030 kg/m^3

parameters of OBWEC are not yet clear.

(2) Power generation efficiency

In addition to the cost factor, power generation efficiency is another important consideration in the commercialization of OBWEC. The power generation by OBWECs needs to go through a conversion process from wave energy to electric energy. The power generation efficiency *PGE* can be expressed by the ratio between the OBWEC's mean power generation $\overline{P}_a$ and the wave power P_d in the area where the OBWEC is located.

$$PGE = \frac{\overline{P}_a}{P_d} \tag{50}$$

$$P_d = \frac{\rho g^2}{32\pi} H_{1/3}^2 T_z D \tag{51}$$

$$\overline{P}_a = \sum_{i=1}^{n} \left| \frac{1}{t_f - t_0} \int_{t_0}^{t_f} \tau_{ai} \dot{\theta}_{ai} dt \right| \tag{52}$$

where ρ, g, $H_{1/3}$, T_z, and D represent seawater density, gravitational acceleration, significant wave height, average wave period, and wave-front device scale, respectively. τ_{ai} and $\dot{\theta}_{ai}$ are the torque and speed of the ith generator of the WECs, respectively.

According to the above analysis, energy cost-efficiency E_{CE} can be defined by combining the OBWEC's scale Q and power generation efficiency *PGE*, as shown in Eq. (53).

$$E_{CE} = \frac{PGE}{Q} \tag{53}$$

It should be noted that Q can approximately represent the OBWEC's investment costs, as shown in the analysis above. Thus, the energy cost-efficiency index E_{CE} indicates the power generation efficiency per unit

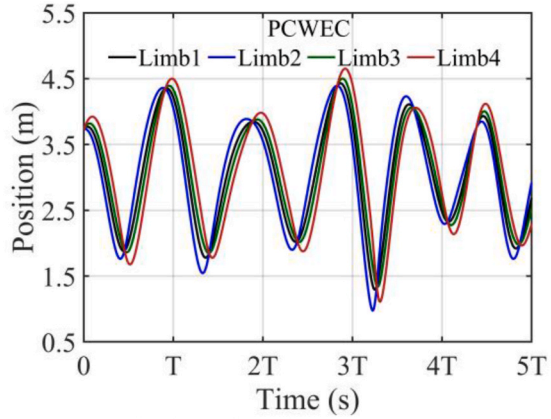

(a) PCWEC limb's position.

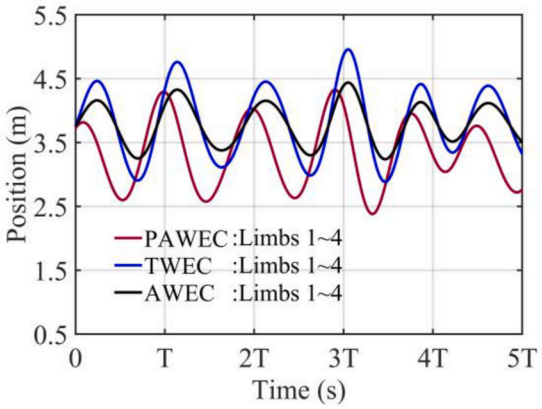

(b) PAWEC, TWEC and AWEC limb's position.

Fig. 13. Power generation limb's position variations for different WECs, in C_{pto} = 40 kN/m, T = 8 s, and $H_{1/3}$ = 2 m.

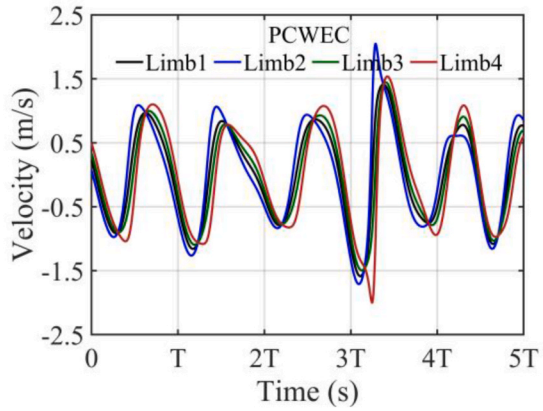

(a) PCWEC limb's velocity.

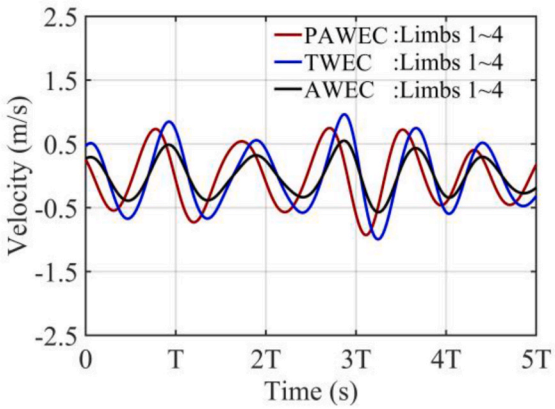

(b) PAWEC, TWEC and AWEC limb's velocity.

Fig. 14. Power generation limb's position variations for different WECs, in C_{pto} = 40 kN/m, T = 8 s, and $H_{1/3}$ = 2 m.

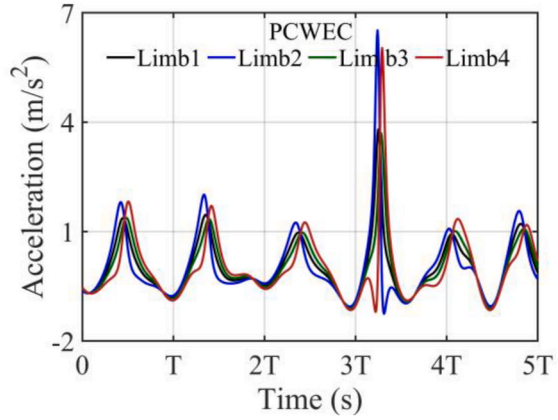

(a) PCWEC limb's acceleration.

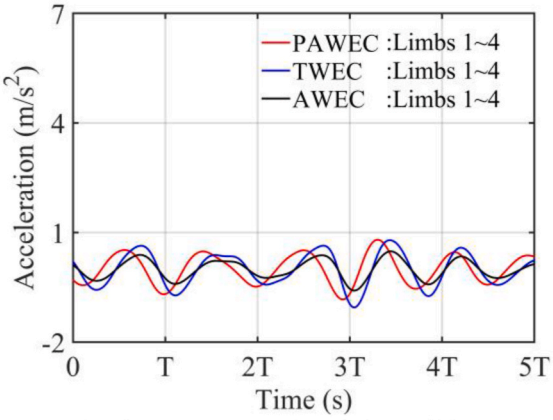

(b) PAWEC, TWEC and AWEC limb's acceleration.

Fig. 15. Power generation limb's acceleration variations for different WECs, in C_{pto} = 40 kN/m, T = 8 s, and $H_{1/3}$ = 2 m.

investment costs of OBWECs. The larger the value of E_{CE}, the greater the development potential of the OBWEC; that is, it can generate as much electricity as possible to supply the grid at a relatively low investment cost, thereby shortening the cost recovery time.

4. Performance comparison and analysis

A WEC must go through a series of performance test stages, including the conceptual design, prototype manufacturing, sea trial and commercial deployment to realize the WEC's engineering application value. Thus, performance analysis is necessary for the PCWEC at the

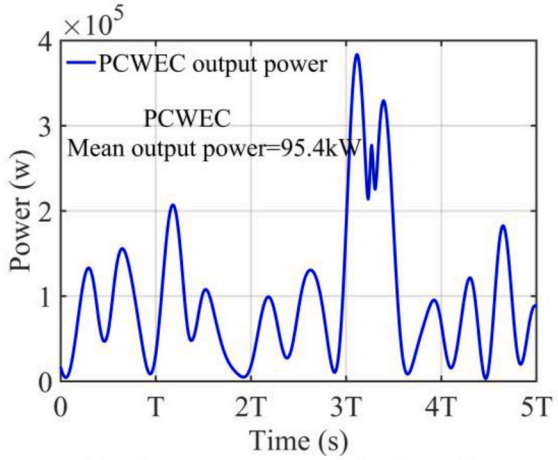

(a) The output power of PCWEC.

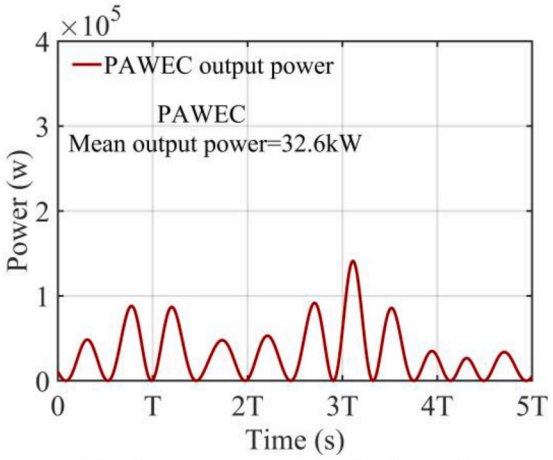

(b) The output power of PAWEC.

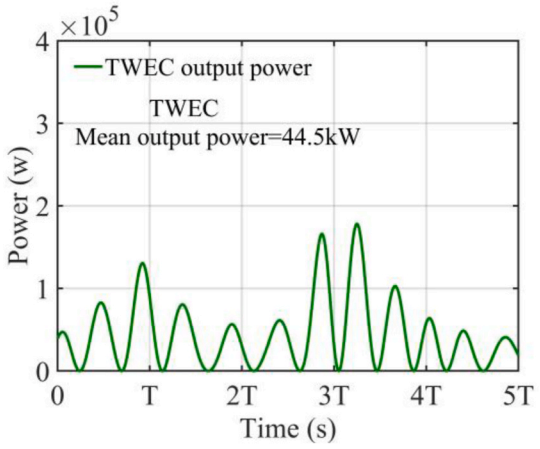

(c) The output power of TWEC.

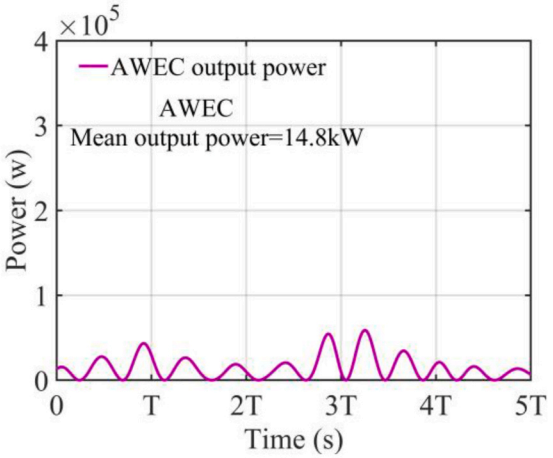

(d) The output power of AWEC.

Fig. 16. The output power of PCWEC, PAWEC, TWEC, and AWEC in C_{pto} = 40 kN/m, T = 8 s, and $H_{1/3}$ = 2 m.

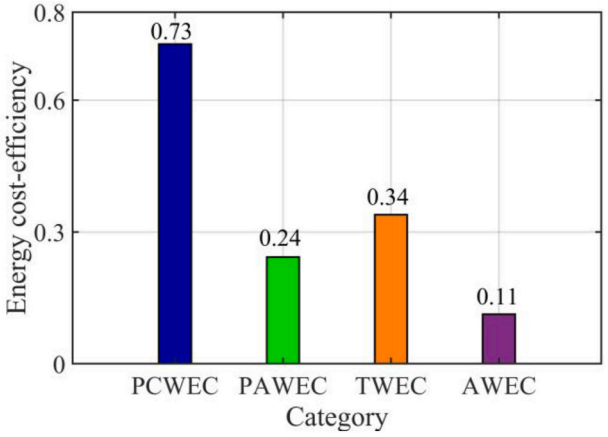

Fig. 17. The energy cost-efficiency of PCWEC, PAWEC, TWEC, and AWEC in C_{pto} = 40 kN/m, T = 8 s, and $H_{1/3}$ = 2 m.

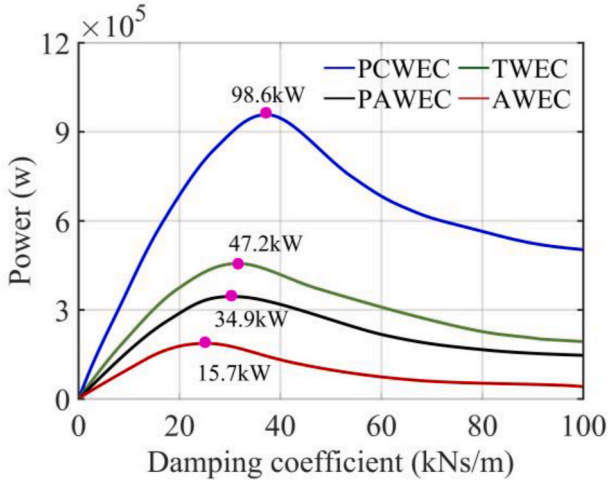

Fig. 18. Effect of PTO damping coefficient (in the range of [0, 100] kNs/m) on the output power for PCWEC, PAWEC, TWEC and AWEC under certain wave states (T = 8 s and $H_{1/3}$ = 2 m).

conceptual design stages to lay the foundation for follow-up research work.

4.1. Case description and model parameterization

The PTO's damping coefficient and wave states have been demonstrated to be important influential factors that could affect the WEC energy conversion [18,19,64]. To conduct the comprehensive analysis of the PCWEC performance, as shown in Fig. 12, we study the

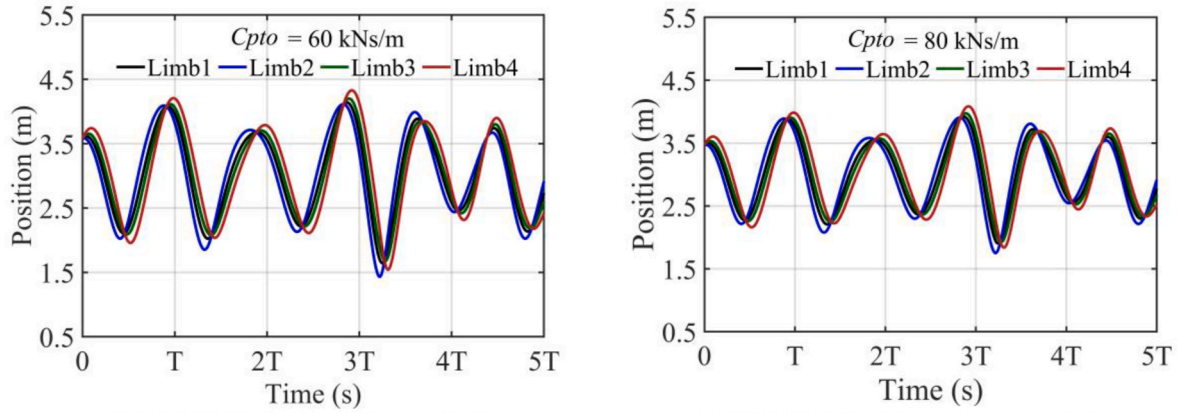

(a) PCWEC limb's position variations in C_{pto}=60 kNs/m, T=8 s, and $H_{1/3}$=2 m.

(b) PCWEC limb's position variations in C_{pto}=80 kNs/m, T=8 s, and $H_{1/3}$=2 m.

Fig. 19. Power generation limb's position variations for PCWEC under different PTO damping coefficients and certain wave states.

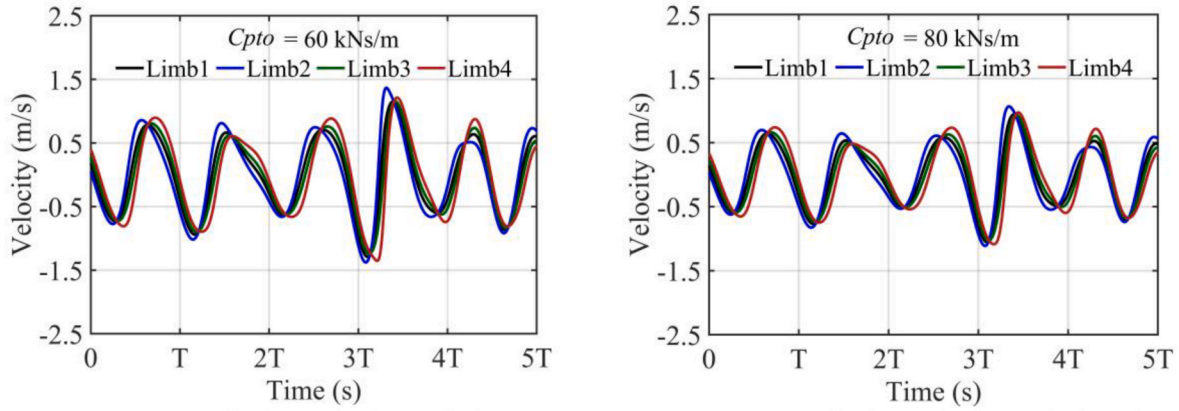

(a) PCWEC limb's velocity variations in C_{pto}=60 kNs/m, T=8 s, and $H_{1/3}$=2 m.

(b) PCWEC limb's velocity variations in C_{pto}=80 kNs/m, T=8 s, and $H_{1/3}$=2 m.

Fig. 20. Power generation limb's velocity variations for PCWEC under different PTO damping coefficients and certain wave states.

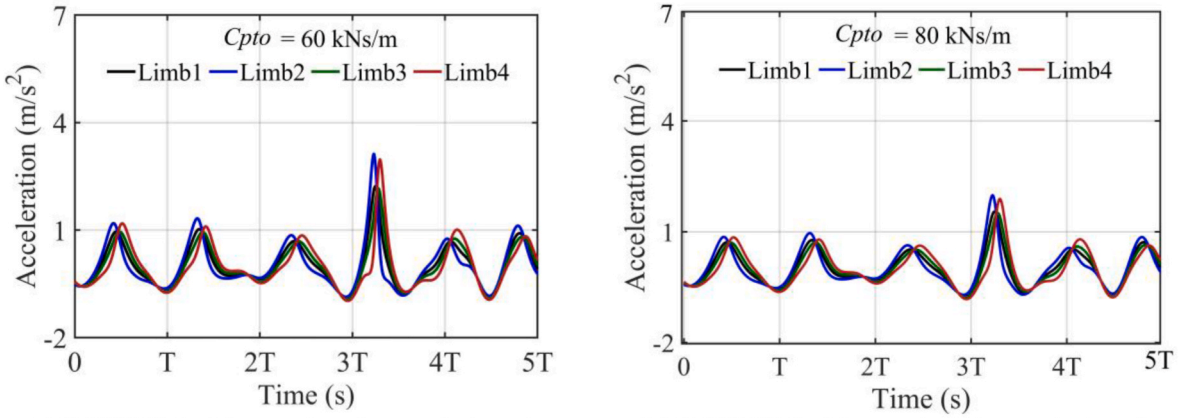

(a) PCWEC limb's acceleration variations in C_{pto}=60 kNs/m, T=8 s, and $H_{1/3}$=2 m.

(b) PCWEC limb's acceleration variations in C_{pto}=80 kNs/m, T=8 s, and $H_{1/3}$=2 m.

Fig. 21. Power generation limb's acceleration variations for PCWEC under different PTO damping coefficients and certain wave states.

energy conversion of PCWEC under different PTO damping coefficients and different wave states and compare it with three typical OBWECs: point absorption WEC (PAWEC), terminator WEC (TWEC), and attenuation WEC (AWEC). Specifically, the three case studies included are: (i) performance comparison under certain parameters, (ii) performance comparison under different PTO parameters and (iii)

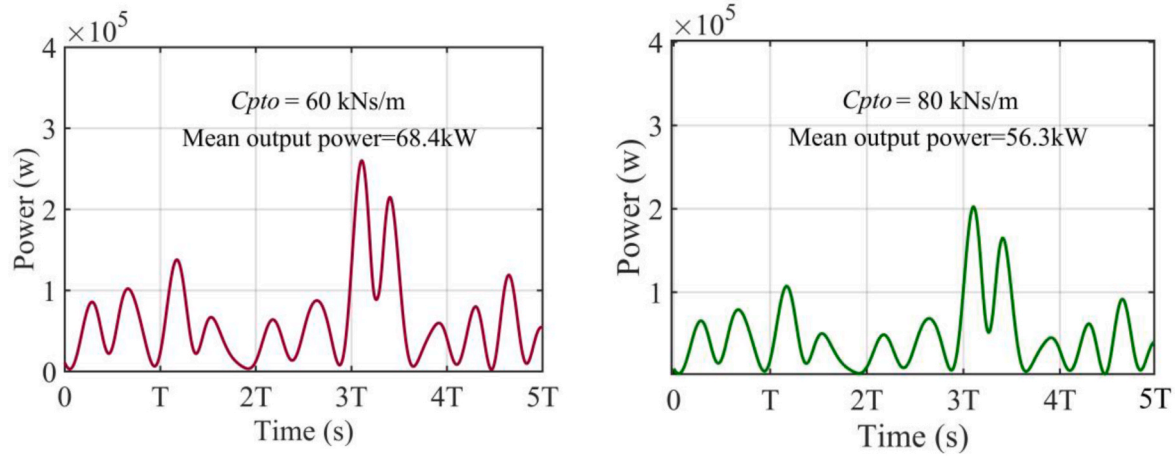

(a) PCWEC's output power in C_{pto}=60 kNs/m, T=8 s, $H_{1/3}$=2 m.

(b) PCWEC's output power in C_{pto}=80 kNs/m, T=8 s, $H_{1/3}$=2 m.

Fig. 22. The output power of PCWEC under different PTO damping coefficients and certain wave states.

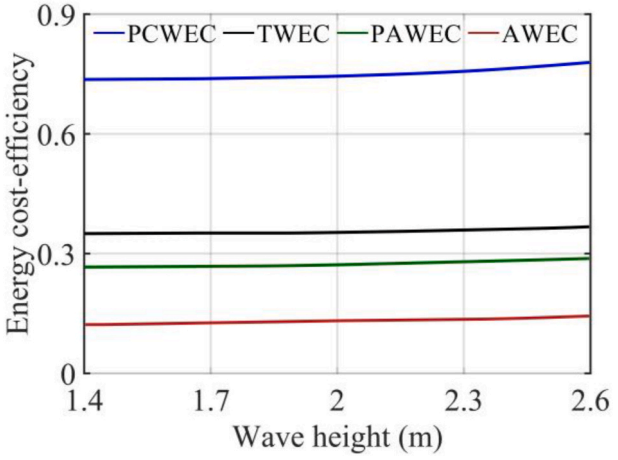

Fig. 23. Effect of different wave heights (in the range of [1.4, 2.6] m) on energy cost-efficiency for PCWEC, PAWEC, TWEC and AWEC, in C_{pto} = 40 kN/m and T = 8 s.

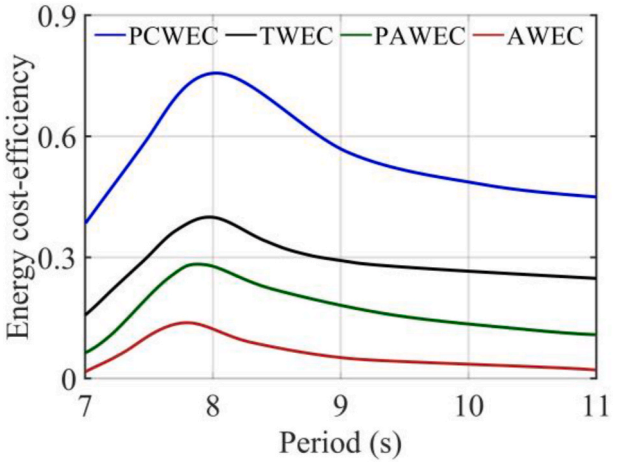

Fig. 24. Effect of different wave periods (in the range of [7,11] s) on energy cost-efficiency for PCWEC, PAWEC, TWEC and AWEC, in C_{pto} = 40 kN/m and $H_{1/3}$ = 2 m.

performance comparison under different wave states.

The dimensions and structural parameters of the PCWEC components are given in Table 4 by the modeling software SOLIDWORKS. The kinematic characteristics of the ocean waves of the northern South China coast are given in Table 5 [65]. Other parameters used for the numerical analysis are Ph = 0.08m and λ = 0.96. The motion equations of the PAWEC, TWEC and AWEC are adopted from Refs. [27–29] and shall not be repeated in this paper. Moreover, to make the performance comparison results more fair, reasonable and credible, in addition to the difference in operation mechanism, the number and structure of PTO and the characteristic structural parameters of the PAWEC, AWEC and TWEC should be consistent with the PCWEC and shall not be repeated here.

4.2. Case results and analysis

4.2.1. Performance comparison under certain parameters

In this case, the PTO's damping coefficient C_{pto}, the wave period T and significant wave height $H_{1/3}$ equal 40 kN/m, 8 s and 2 m, respectively. Figs. 13–15 illustrate that the position, velocity and acceleration variation for PCWEC's power generation limbs are significantly greater than those of the other three OBWECs within the five wave motion periods. Given that the PAWEC can only reciprocate in a single direction, the kinematic response of its four power generation limbs should be consistent. Similarly, the same is true with TWEC and AWEC. The above-mentioned result reveals that PCWEC has a more intense kinematic response than the PAWEC, TWEC and AWEC when the wave states and PTO damping coefficients are certain. These results are expected because the PCWEC has three degrees of freedom to absorb wave forces from three directions. The results of the above kinematic response provide strong evidence for the ability of PCWEC to absorb more wave energy.

Fig. 16 presents the output power of PCWEC, PAWEC, TWEC, and AWEC in C_{pto} = 40 kN/m, T = 8 s and $H_{1/3}$ = 2 m. Compared to the other three WECs, the PCWEC has the highest output power, corresponding to its largest kinematic response, as previously stated. More specifically, the mean output power values within five wave motion periods are 95.4 kW, 32.6 kW, 44.5 kW and 14.8 kW for PCWEC, PAWEC, TWEC, and AWEC, respectively. The PCWEC produces approximately 292.6%, 214.4% and 644.6% more power than PAWEC, TWEC, and AWEC, respectively, benefiting from the fact that PCWEC takes advantage of multiple DOF to improve the energy absorption over their single DOF counterpart. Moreover, Fig. 17 shows that the PCWEC has a much greater energy cost-efficiency than the other three OBWECs, followed by

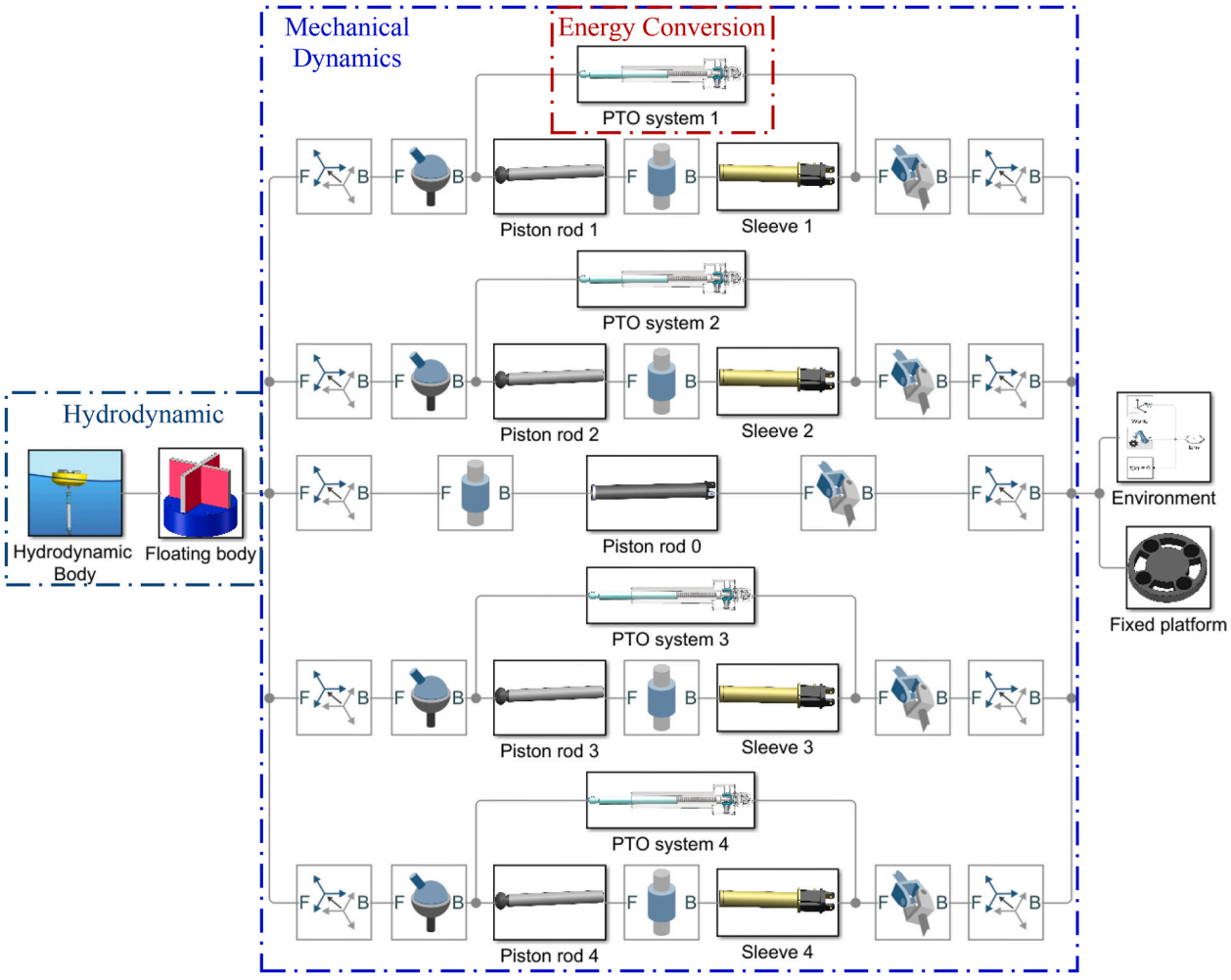

Fig. 25. The simulation system model of the PCWEC.

the TWEC, the PAWEC, and the AWEC. The above analysis exhibits that the proposed PCWEC has a better ability to convert electric energy than the other typical OBWECs under the same device scale because of its structural characteristic with multi DOF.

4.2.2. Performance comparison under different PTO parameters

In this case, we first studied the effects of different PTO damping coefficients C_{pto} (in the range of [0, 100] kNs/m) on the output power of PCWEC, PAWEC, TWEC and AWEC under certain wave states ($T = 8$ s and $H_{1/3} = 2$ m), as shown in Fig. 18. Secondly, we focus on analyzing the kinematic response and output power of PCWEC when the damping coefficient of the PTO is equal to 40, 60 and 80 kN/m.

As shown in Fig. 18, compared with the above three typical OBWECs, the output power of PCWEC is significantly greater under different PTO damping coefficients. Moreover, the optimal output power values are 98.6 kW, 47.2 kW, 34.9 kW and 15.7 kW for PCWEC, PAWEC, TWEC, and AWEC, respectively. The PCWEC produces about 208.9%, 282.5% and 628.1% more power than PAWEC, TWEC, and AWEC through PTO optimum control, respectively, highlighting the potential advantages of the PCWEC structure, which can generate more electric energy than the three typical OBWECs structures.

Figs. 19–21 show the PCWEC limb's position, velocity, and acceleration when the damping coefficient of the PTO is equal to 60 and 80 kN/m. The case of $C_{pto} = 40$ kN/m has been analyzed in Section 4.2.1 and is not repeated. Thus, combined with Fig. 13(a), 14(a) and 15(a) and Figs. 19–21, we can observe that with the increase of the PTO damping coefficient, the PCWEC limb's position, velocity and acceleration all appear significantly reduced. The striking acceleration peak around the 3T environment in Fig. 15a is eliminated to a certain extent by this control method. Considering that excessive acceleration causes a structural impact on the mechanical device, which is harmful to the long-term operation of the OBWEC. Thus, we can lower the possibility of damage to the PCWEC by increasing the PTO damping coefficient. However, in terms of the output power of PCWEC, Figs. 22 and 16a show that, within the five wave motion periods, the output power value of PCWEC when $C_{pto} = 40$ kN/m is significantly larger than that when C_{pto} is equal to 60 and 80 kN/m. The above results reveal that although an excessive PTO damping coefficient can reduce the risk of device damage, it is not beneficial to the power generation of PCWEC. Consequently, comprehensively considering the output power and the impact resistance of PCWEC is necessary when performing PTO control.

4.2.3. Performance comparison under different wave states

Given the randomness of ocean wave motion, an OBWEC with good commercial development potential must maintain high energy cost efficiency under different wave states. In this case, we analyze the impacts of different wave heights (in the range of [1.4, 2.6] m) and different wave periods (in the range of [7,11] s) on the energy cost-efficiency of PCWEC, PAWEC, TWEC and AWEC, as shown in Figs. 23 and 24, respectively. The above wave state data are taken from historical observations over the past five years in the northern South China coast [65].

Fig. 23 shows that the energy cost-efficiency of PCWEC, PAWEC, TWEC and AWEC is less affected by the wave height. Moreover, under

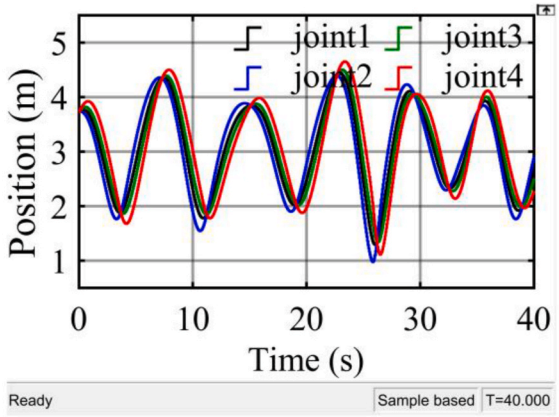

(a) The simulation of PCWEC limb position variations.

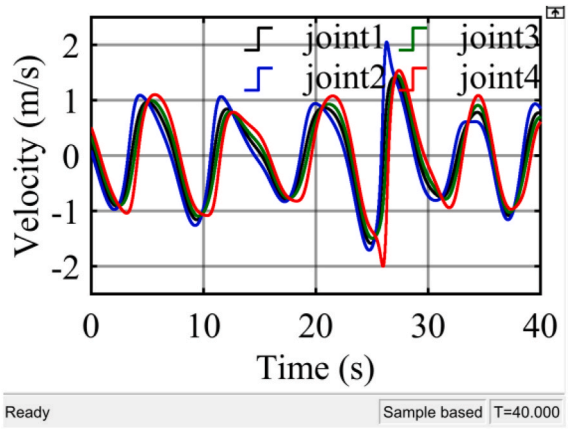

(b) The simulation of PCWEC limb velocity variations.

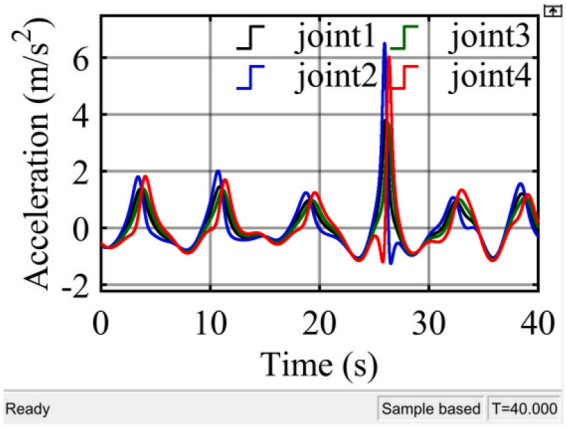

(c) The simulation of PCWEC limb acceleration variations.

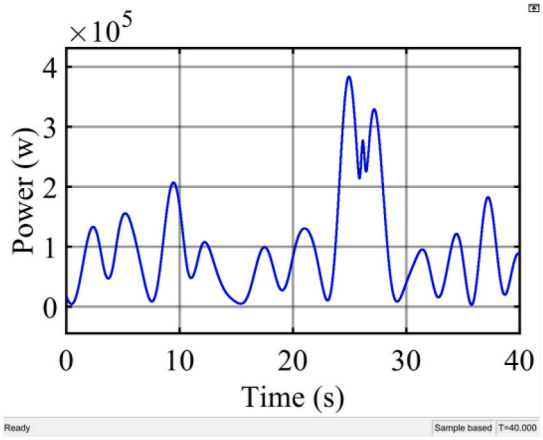

(d) The simulation of PCWEC output power variations.

Fig. 26. The simulation of position, velocity, acceleration and out power vs. time for PCWEC.

different wave heights, the PCWEC has significantly higher energy cost-efficiency than the other three OBWECs. Interestingly, although the wave energy is more affected by the wave height than the wave period according to Eq. (51), we observe by comparing Fig. 23 with Fig. 24 that the wave period has appreciably affected the energy cost-efficiency than wave height for these above four OBWECs. The reason is that the change of the wave period will cause the wave frequency to approach or depart from the natural frequency of OBWEC, thus changing the power generation efficiency of OBWEC in an extensive range. Additionally, Fig. 24 reveals that the PCWEC has significantly greater energy cost-efficiency than the other three OBWECs under different wave periods on this coast. Overall, the above results further highlight the excellent characteristics of PCWEC that can maintain high energy cost-efficiency under changing wave states and confirm that the proposed PCWEC has excellent development potential to promote the commercialization of OBWECs.

5. Simulation

PCWEC is simulated under the irregular wave states shown in Table 5 and compared with the numerical analysis results to verify the correctness of the modeling and analytical results. The model correctness of PAWEC has been extensively verified and will not be simulated here. The PCWEC simulation involves three mutually coupled nonlinear systems: hydrodynamic, mechanical dynamics and energy conversion. Fig. 25 shows the detailed simulation block diagram in Simulink, which illustrates the concrete implementation of the simulation system model of PCWEC.

(1) Regarding hydrodynamics, the Boundary Element Method software WAMIT [62] is used to calculate the time-domain parameters, such as the impulse response function of excitation wave, impulse response function of radiation wave and added mass coefficient. The hydrodynamic body simulation module of WEC-SIM [34,66] is used to analyze the floating body's wave force and moment.
(2) Regarding mechanical dynamics analysis, the SOLIDWORKS and Multibody simulation module in MATLAB is used to import the mechanical structure parameters and construct the constraint relationships among the floating body, the PTO and the fixed platform. The position, velocity and acceleration of each PTO joint are simulated in combination with the external wave force of the floating body.
(3) Regarding energy conversion, the PTO-SIM of WEC-SIM and the multibody simulation module of MATLAB are used to establish the energy conversion model of PTO to obtain the output power of the PCWEC.

The simulation results for the position, velocity, acceleration and output power of PCWEC were obtained by simulation in Simulink, as shown in Fig. 26. By comparing the simulation results in Fig. 26 with the numerical calculation results in Fig. 13(a), 14(a) and 15(a) and Fig. 16a, the trends of the corresponding two curves are the same, thus verifying the correctness of the theoretical modeling for the PCWEC.

6. Conclusions

The lower power generation efficiency of the present oscillating body wave energy converter (OBWEC) severely hinders its commercial development. To this end, the present study attempts to address the above gap by introducing a novel parallel configuration WEC (PCWEC) structure that integrates the multi-degree of freedom (DOF) WEC and parallel mechanical structural characteristics. Moreover, we construct PCWEC's energy conversion model and compare its performance with three typical OBWECs. The key findings from this study are outlined below.

(1) PCWEC has a more intense kinematic response and a higher output power than the point absorption WEC (PAWEC), terminator WEC (TWEC) and attenuation WEC (AWEC) under the same device scale, highlighting the PCWEC concept's advantage over their single DOF counterpart.
(2) Compared with the three typical OBWECs, the optimal output power of PCWEC controlled by power take-off (PTO) is much greater, highlighting the potential advantage of the PCWEC structure that can generate more electric energy.
(3) Increasing the PTO damping coefficient can reduce the PCWEC power generation limb's acceleration and thus lower the possibility of damage to the PCWEC as the structural impact is caused by excessive acceleration. However, an excessive PTO damping coefficient is not beneficial to the power generation of PCWEC. Consequently, the output power and the impact resistance of PCWEC should be comprehensively considered when performing PTO control.
(4) PCWEC is significantly greater in terms of energy cost-efficiency compared with three typical OBWECs, regardless of wave height or wave period variation. Therefore, the excellent characteristics of the PCWEC that can maintain high energy cost-efficiency under changing wave states are highlighted.

In closing, the aforementioned study improves the present OBWEC's power generation performance and application prospects and provides valuable guidance for the structure design and modeling of OBWEC with multi-DOF. Furthermore, the energy cost efficiency metric proposed in this study will also help to evaluate the development potential of different OBWECs, especially in the conceptual design stages. The optimal control concerning output power and impact resistance of the PCWEC is not yet considered in this study, which can also be important to the efficient and reliable operation of PCWEC. However, this idea is beyond the scope of the current study, and we will research it and validate the relative concept of PCWEC using physical model experiments in the future.

CRediT authorship contribution statement

Yongxing Zhang: Writing – original draft, Writing – review & editing. **Zhicong Huang:** Project administration, Supervision, Writing – review & editing. **Bowei Zou:** Investigation, Resources. **Jing Bian:** Supervision.

Declaration of competing interest

The authors declare that they have no known competing financial interests or personal relationships that could have appeared to influence the work reported in this paper.

Acknowledgments

This work was supported by the National Natural Science Foundation of China (Grant No. 52007067) and Guangdong Provincial Natural Science Foundation (Grants No. 2022A1515011581 and No. 2023A1515011623).

References

[1] U.K. Pata, Renewable and non-renewable energy consumption, economic complexity, CO2 emissions, and ecological footprint in the USA: testing the EKC hypothesis with a structural break, Environ. Sci. Pollut. Res. 28 (2021) 846–861.
[2] J. Li, S. Jiang, Energy security in the era of transition, Glob. Energy Interconnect. 2 (2019) 375–377.
[3] R. Ahamed, K. McKee, I. Howard, Advancements of wave energy converters based on power take off (PTO) systems: a review, Ocean Eng. 204 (2020), 107248.
[4] H.P. Nguyen, C.M. Wang, Z.Y. Tay, V.H. Luong, Wave energy converter and large floating platform integration: a review, Ocean Eng. 213 (2020), 107768.
[5] A.F. de O. Falcão, Wave energy utilization: a review of the technologies, Renew. Sustain. Energy Rev. 14 (2010) 899–918.
[6] Y.X. Zhang, Y.J. Zhao, W. Sun, J.X. Li, Ocean wave energy converters: technical principle, device realization, and performance evaluation, Renew. Sustain. Energy Rev. 141 (2021), 110764.
[7] A. Clément, P. McCullen, A. Falcão, A. Fiorentino, F. Gardner, K. Hammarlund, G. Lemonis, T. Lewis, K. Nielsen, S. Petroncini, M.-T. Pontes, P. Schild, B.-O. Sjöström, H.C. Sørensen, T. Thorpe, Wave energy in Europe: current status and perspectives, Renew. Sustain. Energy Rev. 6 (2002) 405–431.
[8] S. Chandrasekaran, V.V.S. Sricharan, Numerical analysis of a new multi-body floating wave energy converter with a linear power take-off system, Renew. Energy 159 (2020) 250–271.
[9] S. Esmaeilzadeh, M.-R. Alam, Shape optimization of wave energy converters for broadband directional incident waves, Ocean Eng. 174 (2019) 186–200.
[10] A. Garcia-Teruel, D.I.M. Forehand, Optimal wave energy converter geometry for different modes of motion, in: Proceedings of the 3rd International Conference on Renewable Energies Offshore (RENEW 2018) - Advances in Renewable Energies Offshore, 2018, pp. 299–305. Lisbon.
[11] W. Zhang, H. Liu, L. Zhang, X. Zhang, Hydrodynamic analysis and shape optimization for vertical axisymmetric wave energy converters, China Ocean Eng. 30 (2016) 954–966.
[12] M. Göteman, Wave energy parks with point-absorbers of different dimensions, J. Fluid Struct. 74 (2017) 142–157.
[13] B. Guo, J.V. Ringwood, Geometric optimisation of wave energy conversion devices: a survey, Appl. Energy 297 (2021), 117100.
[14] A. Maria-Arenas, A.J. Garrido, E. Rusu, G. Izaskun, Control strategies applied to wave energy converters: state of the art, Energies 12 (2019) 3115.
[15] J. Falnes, A. Kurniawan, Ocean Waves and Oscillating Systems: Linear Interactions Including Wave-Energy Extraction, second ed., Cambridge University Press, 2020.
[16] E. Anderlini, D.I.M. Forehand, E. Bannon, M. Abusara, Reactive control of a wave energy converter using artificial neural networks, Int. J. Mar. Energy. 19 (2017) 207–220.
[17] J.C.C. Henriques, L.M.C. Gato, A.F.O. Falcão, E. Robles, F.-X. Faÿ, Latching control of a floating oscillating-water-column wave energy converter, Renew. Energy 90 (2016) 229–241.
[18] L. Li, Y. Gao, D.Z. Ning, Z.M. Yuan, Development of a constraint non-causal wave energy control algorithm based on artificial intelligence, Renew. Sustain. Energy Rev. 138 (2021), 110519.
[19] S. Zhan, G. Li, C. Bailey, Economic feedback model predictive control of wave energy converters, IEEE Trans. Ind. Electron. 67 (2020) 3932–3943.
[20] W. Chen, Z. Wu, J. Liu, Z. Jin, X. Zhang, F. Gao, Efficiency analysis of a 3-DOF wave energy converter (SJTU-WEC) based on modeling, simulation and experiment, Energy 220 (2021), 119718.
[21] D.E. Galván-Pozos, F.J. Ocampo-Torres, Dynamic analysis of a six-degree of freedom wave energy converter based on the concept of the Stewart-Gough platform, Renew. Energy 146 (2020) 1051–1061.
[22] M. Bonovas, K. Belibassakis, E. Rusu, Multi-DOF WEC performance in variable bathymetry regions using a hybrid 3D BEM and optimization, Energies 12 (2019) 2108.
[23] N. Tran, N.Y. Sergiienko, B.S. Cazzolato, B. Ding, P.-Y. Wuillaume, M.H. Ghayesh, M. Arjomandi, On the importance of nonlinear hydrodynamics and resonance frequencies on power production in multi-mode WECs, Appl. Ocean Res. 117 (2021), 102924.
[24] H. Shi, S. Huang, F. Cao, Hydrodynamic performance and power absorption of a multi-freedom buoy wave energy device, Ocean Eng. 172 (2019) 541–549.
[25] W. Chen, F. Gao, X. Meng, Oscillating body design for A 3-DOF wave energy converter, China Ocean Eng. 32 (2018) 453–460.
[26] W. Sheng, Wave energy conversion and hydrodynamics modelling technologies: a review, Renew. Sustain. Energy Rev. 109 (2019) 482–498.
[27] J. Tao, M. Hann, D. Greaves, H. Shi, Numerical study of a point absorber wave energy converter with different power take-off systems, Ocean Eng. 242 (2021), 110181.
[28] D.Z. Ning, B.Y. Ding, Modelling and Optimization of Wave Energy Converters, CRC Press, 2022.
[29] M.R. Dhanak, N.I. Xiros (Eds.), Springer Handbook of Ocean Engineering, Springer International Publishing, Cham, 2016.
[30] R.E. Vasquez, C.D. Crane, J.C. Correa, Kinematic analysis of a planar tensegrity mechanism for wave energy harvesting, in: Latest Advances in Robot Kine-Matics, 2012, pp. 102–114.
[31] Z. Ji, M. Lin, H. He, S. Yang, Analysis of a 6-DOF tensegrity-based water wave energy harvester, Cork, Ireland, in: Proceedings of the 12th European Wave and Tidal Energy Conference Series, vol. 27, 2017. August, 1 September.

[32] N.Y. Sergiienko, B. Cazzolato, M. Arjomandi, An optimal arrangement of mooring lines for the three-tether submerged point-absorbing wave energy converter, Renew. Energy 93 (1) (2016) 27–37.
[33] W. Short, D.J. Packey, T. Holt, A Manual for Economic Evaluation of Energy Efficiency and Renewable Energy Technologies, NREL, 1995. NREL/TP-462-5173.
[34] S. Chandrasekaran, V.V.S. Sricharan, Numerical study of bean-float wave energy converter with float number parametrization using WEC-Sim in regular waves with the Levelized Cost of Electricity assessment for Indian sea states, Ocean Eng. 237 (2021), 109591.
[35] L. Castro-Santos, G.P. Garcia, A. Estanqueiro, P.A.P.S. Justino, The Levelized Cost of Energy (LCOE) of wave energy using GIS based analysis: the case study of Portugal, Int J Elec Power 65 (2015) 21–25.
[36] A. De Andres, R. Guanche, C. Vidal, I.J. Losada, Adaptability of a generic wave energy converter to different climate conditions, Renew. Energy 78 (2015) 322–333.
[37] IEA & NEA, Projected Price of Generating Electricity, UE, 2010.
[38] J. You, F. Xi, H. Shen, J. Wang, X. Yang, A novel Stewart-type parallel mechanism with topological reconfiguration: design, kinematics and stiffness evaluation, Mech. Mach. Theor. 162 (2021), 104329.
[39] M. Chen, Q. Zhang, X. Qin, Y. Sun, Kinematic, dynamic, and performance analysis of a new 3-DOF over-constrained parallel mechanism without parasitic motion, Mech. Mach. Theor. 162 (2021), 104365.
[40] Y. Zhao, F. Gao, Dynamic formulation and performance evaluation of the redundant parallel manipulator, Robot. Comput.-Integr. Manuf. 25 (2009) 770–781.
[41] H.D. Taghirad, Parallel Robots: Mechanics and Control, 1nd ed., CRC press, 2013.
[42] M. Penalba, I. Touzón, J. Lopez-Mendia, V. Nava, A numerical study on the hydrodynamic impact of device slenderness and array size in wave energy farms in realistic wave climates, Ocean Eng. 142 (2017) 224–232.
[43] H. Liu, F. Yan, F. Jing, J. Ao, Z. Han, F. Kong, Numerical and experimental investigation on a moonpool-buoy wave energy converter, Energies 13 (2020) 2364.
[44] Y. Wen, W. Wang, H. Liu, L. Mao, H. Mi, W. Wang, G. Zhang, A shape optimization method of a specified point absorber wave energy converter for the South China sea, Energies 11 (2018) 2645.
[45] S. Jin, R.J. Patton, B. Guo, Enhancement of wave energy absorption efficiency via geometry and power take-off damping tuning, Energy 169 (2019) 819–832.
[46] N.Y. Sergiienko, B.S. Cazzolato, B. Ding, P. Hardy, M. Arjomandi, Performance comparison of the floating and fully submerged quasi-point absorber wave energy converters, Renew. Energy 108 (2017) 425–437.
[47] C.E. Clark, A. Garcia-Teruel, B. DuPont, D. Forehand, Towards reliability-based geometry optimization of a point-absorber with PTO reliability objectives, in: Proceedings of European Wave and Tidal Energy Conference, 2019, p. 11.
[48] M.N. Berenjkoob, M. Ghiasi, C.G. Soares, Influence of the shape of a buoy on the efficiency of its dual-motion wave energy conversion, Energy 214 (2021), 118998.
[49] J. Wu, Y. Yao, W. Li, L. Zhou, M. Göteman, Optimizing the performance of solo duck wave energy converter in tide, Energies 10 (2017) 289.
[50] A.J. Caska, T.D. Finnigan, Hydrodynamic characteristics of a cylindrical bottom-pivoted wave energy absorber, Ocean Eng. 35 (2008) 6–16.
[51] H. Zhao, Z. Sun, C. Hao, J. Shen, Numerical modeling on hydrodynamic performance of a bottom-hinged flap wave energy converter, China Ocean Eng. 27 (2013) 73–86.
[52] L. Papillon, L. Wang, N. Tom, J. Weber, J. Ringwood, Parametric modelling of a reconfigurable wave energy device, Ocean Eng. 186 (2019), 106105.
[53] A. Kurniawan, T. Moan, Optimal geometries for wave absorbers oscillating about a fixed Axis, IEEE J. Ocean. Eng. 38 (2013) 117–130.
[54] J. Zhang, Z. Jin, H. Feng, Type synthesis of a 3-mixed-DOF protectable leg mechanism of a firefighting multi-legged robot based on GF set theory, Mech. Mach. Theor. 130 (2018) 567–584.
[55] J. Yang, F. Gao, Q.J. Ge, X. Zhao, W. Guo, Z. Jin, Type synthesis of parallel mechanisms having the first class GF sets and one-dimensional rotation, Robotica 29 (2011) 895–902.
[56] C.H. Kuo, J.S. Dai, Task-oriented structure synthesis of a class of parallel manipulators using motion constraint generator, Mech. Mach. Theor. 70 (2013) 394–406.
[57] R. Lin, W. Guo, S.S. Cheng, Type synthesis of 2R1T remote center of motion parallel mechanisms with a passive limb for minimally invasive surgical robot, Mech. Mach. Theor. 172 (2022), 104766.
[58] H.-C. von Seherr-Thoss, F. Schmelz, E. Aucktor, F. Schmelz, H.-C. von Seherr-Thoss, Universal Joints and Driveshafts: Analysis, Design, Applications, Springer, Berlin Heidelberg, 2006.
[59] B. Siciliano, O. Khatib (Eds.), Springer Handbook of Robotics, Springer International Publishing, Cham, 2016.
[60] Y. Li, M. Lin, Regular and irregular wave impacts on floating body, Ocean Eng. 42 (2012) 93–101.
[61] X. Ji, E.A. Shami, J. Monty, X. Wang, Modelling of linear and non-linear two-body wave energy converters under regular and irregular wave conditions, Renew. Energy 147 (2020) 487–501.
[62] A. Albert, G. Berselli, L. Bruzzone, P. Fanghella, Mechanical design and simulation of an onshore four-bar wave energy converter, Renew. Energy 114 (2017) 766–774.
[63] W.E. Cummins, W. Iiuhl, A. Uinm, The impulse response function and ship motions, Schiffstechnik 9 (1962) 101–109.
[64] M. Folley, T.J.T. Whittaker, The effect of sub-optimal control and the spectral wave climate on the performance of wave energy converter arrays, Appl. Ocean Res. 31 (2009) 260–266.
[65] National Science & Technology Infrastructure, Measured data, Available at: http://mds.nmdis.org.cn/.
[66] V.V.S. Sricharan, S. Chandrasekaran, Time-domain analysis of a bean-shaped multi-body floating wave energy converter with a hydraulic power take-off using WEC-Sim, Energy 223 (2021), 119985.